Analysis of the Blade Element Momentum Theory

Jeremy Ledoux, Sebastián Riffo, Julien Salomon

ANALYSIS OF THE BLADE ELEMENT MOMENTUM THEORY

JEREMY LEDOUX*, SEBASTIÁN RIFFO*, AND JULIEN SALOMON†

Abstract. The Blade Element Momentum theory (BEM), introduced by H. Glauert in 1926, provides a framework to model the aerodynamic interaction between a turbine and a fluid flow. This theory is either used to estimate turbine efficiency or as a design aid. However, a lack of mathematical interpretation limits the understanding of some of its angles. The aim of this paper is to propose an analysis of BEM equations. Our approach is based on a reformulation of Glauert's model which enables us to identify criteria which ensure the existence of solution(s). In this framework, we also study the convergence of solution algorithms and analyze turbine design procedures. The mathematical analysis is completed and illustrated by numerical experiments.

Key words. Turbine design, Blade Element Momentum theory, Computational Fluid Dynamics, Geometry Modeling, Wind Turbine Aerodynamics, Fluid–Structure Interaction

AMS subject classifications. 76G25, 76M99, 65Z05

1. Introduction.

The *Blade Element Momentum* (BEM) *theory* is a model used to evaluate the performance of a propelling or extracting turbine on the basis of its mechanical and geometric parameters as well as the characteristics of the interacting flow. This model results from the combination of two theories: the *Blade Element Theory* and the *Momentum Theory*. The former was introduced by William Froude [10] in 1878 to study the behavior of turbines from a local point of view. In this framework, the turbine blade is cut into sections, the *blade elements*, each of them being approximated by a planar model. This approach results in expressions of the forces exerted on the blade element, as functions of the flow characteristics and blade geometry. The fundamental quantities of this model are two experimental coefficients (usually denoted by C_L and C_D), called *lift* and *drag coefficients* respectively, which account for the forces in the cross-section as functions of the *angle of attack*, i.e. the relative angle between the rotating blade and flow. The results are then integrated along the blade to obtain global values.

The Momentum Theory, also known as *Disk Actuator Theory* or *Axial Momentum Theory*, was introduced by William J. M. Rankine in 1865 [25] and is, unlike the Blade Element Theory, a global theory that adopts a macroscopic point of view to model the behavior of a column of fluid passing through a turbine. This approach was later taken up independently by Frederick W. Lanchester [20], Albert Betz [3] and Nikolay Joukowsky [18, 19], to formulate *Betz's Law*, which gives the theoretical optimal efficiency of a thin rotor, see [31]. A combination of these two approaches was carried out in 1926 by Hermann Glauert [13], who also refined the Momentum Theory by taking into account the rotation of the fluid rings induced by its interaction with the turbine.

The resulting Blade Element Momentum theory is thus based two decompositions: (i) a radial decomposition of the blades and the fluid column, considered as concentric rings that do not interact with each other, and (ii) a decomposition of the fluid/turbine system into a macroscopic part via Momentum Theory and a local planar part via Blade Element Theory. Such a description of Glauert's theory is given

*CEREMADE, CNRS, UMR 7534, Université Paris-Dauphine, PSL University, France (ledoux@ceremade.dauphine.fr,sebastian.reyes-riffo@dauphine.eu).

†INRIA Paris, ANGE Project-Team, 75589 Paris Cedex 12, France and Sorbonne Université, CNRS, Laboratoire Jacques-Louis Lions, 75005 Paris, France (julien.salomon@inria.fr).

in the monographs [5, 7, 14, 22, 26, 29, 30], see for example [29, p.100] :

"In the BEM theory, the loading is computed using two independent methods, by combining a local blade-element consideration, using tabulated two-dimensional airfoil data, with the one-dimensional momentum theorem."

or [14, p.56] :

"The Blade Element Momentum method couples the momentum theory with the local events taking place at the actual blades. The stream tube introduced in the 1-D momentum theory is discretized into N annular elements"

Though old, Glauert's model is still currenty used to evaluate turbine efficiency, as indicated in [29, p.23]:

"Although a variety of correction models have been developed since then [...], the model based on the momentum theory by Glauert (1935) still remains one, the most popular."

This longevity can be partly explained by the relative simplicity of the approach compared to the complex phenomenon that develops in the coupled turbine/fluid system. This time dependent 3D-fluid/structure interaction problem is indeed a major modeling challenge, which BEM reduces to static 0D and 2D-computations. With this, the main computational effort consists of solving (2D-)partial differential equations, typically stationary Navier-Stokes, or, more often than not, of using experimental data from wind tunnel profile tests. Let us add that the numerical efficiency of this method is all the more crucial as turbine models are mostly implemented as part of design procedures, through iterative optimization loops. In practice, this means that equations have to be solved many times and only simple formulations such as BEM allows the designer to carry out the computations to a satisfactory point, or at least to provide a good enough initial guess for a finer design, as pointed out in [23, p.2]:

"Blade element momentum theory continues to be widely used for wind turbine applications such as initial aerodynamic analysis, conceptual design, loads and stability analysis, and controls design."

Note that other models have been proposed, such as Joukowsky's model [17] where the axial wake velocity is assumed to be constant. This model, experimentally deficient in some conditions, is not widely used. The significant increase in computational power as well as the theoretical advances obtained in the field of fluid-structure interaction simulation now also make it possible to simulate 3D models based on the Navier-Stokes equation [1, 2, 16], or to include BEM in larger models, as Lagrangian stochastic solvers see [4]. Note finally that similar theories have been developped to model vertical axis turbines (of Darreius type) [9].

The purpose of this article is to analyze the Blade element momentum theory from a mathematical point of view. The results we obtain in the course of this analysis will elucidate issues related to the well-posedness of the model, the numerical solution of its equations and the optimality of a blade design. They concern two versions of Glauert's model, which we call *Simplified model* and *Corrected model*. The former allows us to illustrate the main features of our approach, whereas the latter includes some corrections usually considered to remedy the mismatch between the simplified model and experimental observations.

The paper is structured as follows: Section 2 provides a brief exposition of the derivation of the model. We then focus on the resulting algebraic system. The key point of our analysis is to look deeper into Glauert's macroscopic-local decomposition to reformulate these equations into a single equation containing two very distinct terms: a universal term, independent of the turbine under consideration and associated with the macroscopic part of the model, and an experimental term, which

depends on the characteristics of the blades and is associated with the local part of the model. In this context, we show that solving the equations associated with Glauert's model actually means finding an angular value that makes these two terms equal. This result agrees with some implicit conclusions reported before that were not formalized mathematically and rather used for pedagogic purpose, such as in [22, Figure 3.27, p.126]. In contrast, our analysis gives rise to new theoretical and numerical results. In Section 3, our reformulation enables us to identify explicitly which assumptions related to the turbine parameters can guarantee the existence of a solution. In addition, we obtain a classification of multiple solution cases based on the modeling assumptions. In Section 4, we present the usual solution algorithm and derive from our approach more efficient procedures. As already mentioned, BEM is also used in turbine design, where the simplified model is included in a specific optimization method. We recall the details of the resulting procedure in Section 5 and describe an optimization algorithm for the corrected model. We finally present some numerical experiments in Section 6.

Most of our results are based on assumptions related to physical parameters, e.g., on the coefficients C_D and C_L. We do not claim these assumptions always are necessary. However, we treat C_D and C_L as generic functions (endowed with general properties), hence it is often possible to find examples which make our assumptions optimal.

In what follows, we denote by $\mathbb{R}^+$ and $\mathbb{R}^-$ the sets of positive real numbers and non-positive real numbers, respectively.

2. The blade element momentum theory. In this section, we present the model proposed by Glauert to describe the interaction between a turbine and a flow. After having introduced the relevant variables, we recall the main steps of the reasoning leading to the equations of the model. We then detail the two versions of the model considered in this paper.

2.1. Variables. The theory introduced by Glauert aims to establish algebraic relations that characterize the interaction between a flow and a rotating blade, named *turbine* in what follows. In this way, Glauert's model couples two descriptions: a global macroscopic model that describes the evolution of fluids rings crossing the turbine, and a local one, that summarizes in 2D the behavior of a section of a blade, *a blade element*, under the action of the fluid.

The flow is supposed to be horizontal, constant in time and incompressible. The last assumption implies that the flow velocities in the left and right neighborhoods of the turbine have a same value U_0. We denote by $U_{-\infty}$ and $U_{+\infty}$ the upstream and downstream velocities, respectively. As the BEM model does not take into account interactions between blade elements, we restrict ourselves without loss of generality to a fixed blade element and a constant rotation speed Ω, i.e. fixed value of the parameter

$$\lambda := \frac{\Omega r}{U_{-\infty}},$$

where r is the distance of the element to the rotation axis. In practical cases, the turbine works "*at constant lambda*": Ω is indeed often controlled through the torque exerted by a generator in such a way that the ratio $\frac{\Omega}{U_{-\infty}} = \lambda$ is kept constant for various values of $U_{-\infty}$. It follows that the value of λ associated with one element only depends on r. In the sequel, we consequently only use the variable λ to describe the location of a blade element.

2.1.1. Macroscopic variables and BEM unknowns. Glauert's model ultimately consists of a system which links together three variables a, a' and φ associated with a ring of fluid. The two former are usually called the *axial* and *angular induction factor* respectively. They are defined by

$$a = \frac{U_{-\infty} - U_0}{U_{-\infty}}, \tag{2.1}$$

$$a' = \frac{\omega}{2\Omega}, \tag{2.2}$$

where ω is the rotation speed of the considered ring of fluid. The angle φ is the *relative angle deviation* (see [22, p.120]) of the ring, meaning that:

$$\tan\varphi = \frac{1-a}{\lambda(1+a')}. \tag{2.3}$$

For the sake of simplicity, and to emphasize their role of unknowns in Glauert's model, we omit in this paper the dependence of a, a', φ (and α in what follows) on λ in notation.

2.1.2. Local variables. Let us denote by U_{rel} the relative fluid speed (also called *apparent fluid speed*) perceived from this blade element while rotating. By definition of φ, we have:

$$U_{rel} = \frac{U_0}{\sin\varphi}. \tag{2.4}$$

For a given blade profile, the *lift* and *drag coefficients* C_L and C_D are defined through the relations

$$dL = C_L(\alpha)\frac{1}{2}\rho U_{rel}^2 c_\lambda dr,$$
$$dD = C_D(\alpha)\frac{1}{2}\rho U_{rel}^2 c_\lambda dr,$$

where ρ is the mass density of the fluid, dL and dD are the elementary lift and drag forces applying to a blade element of thickness dr and of chord $c_\lambda = c_\lambda(r)$. The parameter α is called *angle of attack* and defined as the angle between the chord and flow direction, hence satisfies the relation

$$\alpha = \varphi - \gamma_\lambda, \tag{2.5}$$

where $-\pi/2 < \gamma_\lambda < \pi/2$ is the *twist* (also called *local pitch*) angle of the blade. The parameters associated with a blade element are summarized in Figure 2.1.

The coefficients C_L and C_D correspond to the ratio between the lift and drag forces and the dynamic force, i.e., the force associated with the observed kinetic energy. They are determined by the profile. Once this one is fixed, the main design parameters are the chord c_λ and the twist γ_λ. Their optimization is discussed in Section 5.

The coefficients C_L and C_D are assumed to be known as functions of α and occasionally of Reynolds number (Re). The latter case is indeed rarely considered in the monographs, where Re is assumed to be constant with respect to α as soon as $U_{-\infty}$, λ, Ω, c_λ are fixed. For the sake of simplicity, we also neglect the changes in

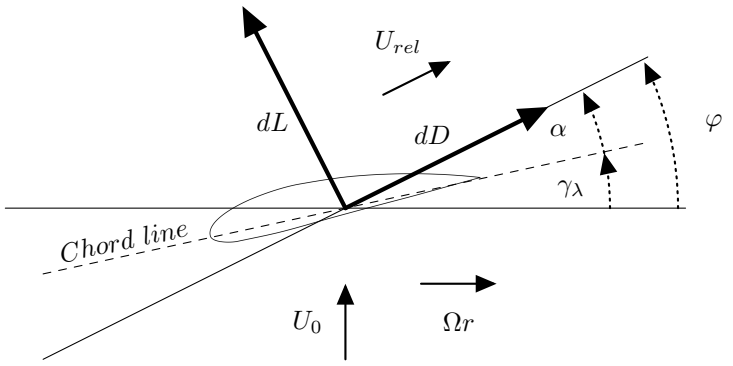

Figure 2.1: Blade element profile and associated angles, velocities and forces.

Re in this paper. However, our results can be extended to non-constant Reynolds numbers [30, p.374-375], i.e. in situations where the functions $(\alpha, Re) \mapsto C_L(\alpha, Re)$ and $\alpha \mapsto C_D(\alpha, Re)$ have to be taken into account. Indeed, Reynolds number is a function of U_{rel}, i.e. of α, see Equations (2.4) and (2.5). We consequently remain in a setting where C_L and C_D are functions of the only variable α. Examples of variations of C_L and C_D with respect to Reynolds number are given in [7, p.169].

Though changing from one profile to another, the behaviors of C_L and C_D as functions of α can be described qualitatively in a general way. The coefficient C_L usually increases nearly linearly with respect to α up to a given critical angle α_s, with $0 < \alpha_s < \pi/2$, where the so-called *stall* phenomenon occurs: C_L then decreases rapidly (see, e.g., [5, p.93-94] and [30, p.375]), causing a sudden loss of lift. For C_D is associated with a drag force, it is always positive and defined for all angles. In general, this coefficient slightly increases in α up to $\alpha = \alpha_s$, and then it becomes very large. It follows then that the condition $\varphi - \gamma_\lambda < \alpha_s$ is always required in the blade design phase. To be coherent with this framework, we summarize the properties of C_L and C_D required for our study by the following assumption.

ASSUMPTION 1. *For some $\beta \in (0, \alpha_s)$, the function $\alpha \mapsto C_L(\alpha)$ is continuous on*

$$I_\beta := [-\beta, \beta],$$

and positive on $I_\beta \cap \mathbb{R}^+$. The function $\alpha \mapsto C_D(\alpha)$ is defined, continuous and non-negative on $\mathbb{R}$.

2.2. Glauert's modeling. For the sake of completeness, we now shortly recall the reasoning proposed by Glauert to model the interaction between a turbine and a flow. We refer to [7, Chap. 3], for a more extended presentation of this theory. We denote by dT and dQ the infinitesimal thrust and torque that apply on the blade element of thickness dr under consideration.

2.2.1. Macroscopic approach. The first part of the model is related to the Momentum Theory and deals with the macroscopic evolution of a ring of fluid. It aims to express dT and dQ in terms of a, a' and φ.

Denote by p_- and p_+ the fluid pressures on the left and right neighborhoods of the blade respectively. Applying Bernouilli's relation between $-\infty$ and 0^- and between

0^+ and $+\infty$ gives rise to

$$p_- - p_+ = \frac{1}{2}\rho(U_{-\infty}^2 - U_{+\infty}^2).$$

Considering then the rate of change of momentum on both sides of the turbine, we get a second expression for the variation in the pressure, namely:

$$p_- - p_+ = \rho(U_{-\infty} - U_{+\infty})U_0.$$

Combining the two previous equations and using (2.1), we obtain:

$$U_{+\infty} = (1-2a)U_{-\infty}.$$

Since $dT = (p_- - p_+)\pi r dr$ and $dQ = \omega\rho U_0 2\pi r^3 dr$, we finally get

$$dT = 4a(1-a)U_{-\infty}^2\rho\pi r dr, \tag{2.6}$$

$$dQ = 4a'(1-a)\lambda U_{-\infty}^2\rho\pi r^2 dr. \tag{2.7}$$

The quantity

$$C_T = \frac{dT}{\frac{1}{2}U_{-\infty}^2\rho 2\pi r dr} = 4a(1-a), \tag{2.8}$$

appearing in (2.6) is often called *local thrust coefficient* [32].

2.2.2. Local approach. Another set of equations can be obtained through the Blade Element Theory, where local expressions for infinitesimal thrust and torque are considered. The approach can be summarized as follows: using (2.5), we find that:

$$dT = \frac{B}{2}U_{rel}^2\left(C_L(\varphi-\gamma_\lambda)\cos\varphi + C_D(\varphi-\gamma_\lambda)\sin\varphi\right)\rho c_\lambda dr,$$
$$dQ = \frac{B}{2}U_{rel}^2\left(C_L(\varphi-\gamma_\lambda)\sin\varphi - C_D(\varphi-\gamma_\lambda)\cos\varphi\right)\rho c_\lambda r dr,$$

where B is the number of blades of the turbine under consideration. These equations can then be combined with (2.4) to give

$$dT = \sigma_\lambda\frac{(1-a)^2}{\sin^2\varphi}\left(C_L(\varphi-\gamma_\lambda)\cos\varphi + C_D(\varphi-\gamma_\lambda)\sin\varphi\right)U_{-\infty}^2\rho\pi r dr, \tag{2.9}$$

$$dQ = \sigma_\lambda\frac{(1-a)^2}{\sin^2\varphi}\left(C_L(\varphi-\gamma_\lambda)\sin\varphi - C_D(\varphi-\gamma_\lambda)\cos\varphi\right)U_{-\infty}^2\rho\pi r^2 dr, \tag{2.10}$$

with

$$\sigma_\lambda = \frac{Bc_\lambda}{2\pi r}. \tag{2.11}$$

2.2.3. Combination of local and global approaches . To get a closed system of equations, Glauert combined the results of the two last subsections. More precisely, equating (2.6) and (2.7) with (2.9) and (2.10) respectively, and dividing both resulting equations by $4(1-a)^2$ gives:

$$\frac{a}{1-a} = \frac{\sigma_\lambda}{4\sin^2\varphi}\left(C_L(\varphi-\gamma_\lambda)\cos\varphi + C_D(\varphi-\gamma_\lambda)\sin\varphi\right) \tag{2.12}$$

$$\frac{a'}{1-a} = \frac{\sigma_\lambda}{4\lambda\sin^2\varphi}\left(C_L(\varphi-\gamma_\lambda)\sin\varphi - C_D(\varphi-\gamma_\lambda)\cos\varphi\right). \tag{2.13}$$

The system obtained by assembling (2.3), (2.12) and (2.13) is the basis of Glauert's Blade Element Momentum theory.

2.3. Simplified model. In the monographs devoted to aerodynamics of wind turbines, the contribution of C_D is sometimes set to zero. This point is discussed in [29, p.135], where it is particular stated:

"Since the drag force does not contribute to the induced velocity physically, C_D is usually omitted when calculating induced velocities.".

In the same way, Manwell and co-authors mention in [22, p.125]:

"In the calculation of induction factors,[...] accepted practice is to set C_D equal to zero [...]. For airfoils with low drag coefficients, this simplification introduces negligible errors."

This assumption is actually justified in many cases, since the procedures used to design profiles aim to minimize their drag. As a matter of fact, the usual blade design procedure starts by selecting a twist angle γ_λ minimizing the ratio $\frac{C_D}{C_L}$, see Section 5.1.

We also consider the case where $C_D = 0$, and referred to as *simplified model* in the following. In view of (2.3), (2.12) and (2.13), it corresponds to the three equations:

$$\tan\varphi = \frac{1-a}{\lambda(1+a')} \tag{2.14}$$

$$\frac{a}{1-a} = \frac{1}{\sin^2\varphi}\mu_L(\varphi)\cos\varphi \tag{2.15}$$

$$\frac{a'}{1-a} = \frac{1}{\lambda\sin\varphi}\mu_L(\varphi), \tag{2.16}$$

where we have introduced the dimensionless function:

$$\mu_L(\varphi) := \frac{\sigma_\lambda}{4}C_L(\varphi-\gamma_\lambda), \tag{2.17}$$

which is defined on

$$I_{\beta,\gamma_\lambda} := [-\beta+\gamma_\lambda, \beta+\gamma_\lambda] \tag{2.18}$$

by virtue of Assumption 1.

2.4. Corrected model. To get closer to experimental results, many modifications of the model defined by (2.3), (2.12) and (2.13) have been introduced, see e.g. [29, Chapter 7]. Hereafter, we present three important corrections, namely non-zero drag coefficient C_D, tip loss correction and a specific treatment of a for cases where its value becomes large. The first and the last will modify significantly the analysis developed for the simplified Glauert's model.

2.4.1. Slowly increasing drag. In addition to consider C_D strictly positive, we shall assume in some parts of the analysis a slow increasing of this parameter before the occurrence of the stall phenomenon.

2.4.2. Tip loss correction. The equations of Momentum Theory are derived assuming that the force from the blades on the flow is constant in each annular element. Such a framework corresponds to a rotor with an infinite number of blades. However, in real life situations, a modification of the flow at the tip of a blade has to be included to take into account that the circulation of the fluid around the blade must go down (exponentially) to zero when $r \to R$. In this way, given a number of blades B and a radius R of the considered turbine, Glauert (see [12, p.268]) has used

the Prandtl tip function F_λ [24]:

$$F_\lambda(\varphi) := \frac{2}{\pi}\cos^{-1}\left(\exp(-\frac{B/2(1-\frac{\lambda U_{-\infty}}{\Omega R})}{(\frac{\lambda U_{-\infty}}{\Omega R})\sin\varphi})\right) = \frac{2}{\pi}\cos^{-1}\left(\exp(-\frac{B/2(1-r/R)}{(r/R)\sin\varphi})\right),$$

as an additional factors in Equations (2.6) and (2.7). This modification gives rise to

$$dT = 4a(1-a)F_\lambda(\varphi)U_{-\infty}^2\rho\pi r dr, \tag{2.19}$$

$$dQ = 4a'(1-a)F_\lambda(\varphi)U_{-\infty}\rho\pi r^3\Omega dr. \tag{2.20}$$

Further models of tip loss corrections have been introduced in between. We refer to [5, Chap. 13] and [27] for reviews of these approaches.

2.4.3. Correction for high values of a. For induction factors a larger than about 0.4 (see [30, p.297]), a turbulent wake generally appears, and it is broadly considered that momentum theory does not apply. This fact was already noted by Glauert (see [11]), who proposed to modify the thrust expression (2.8) for values of a larger than a fixed threshold value a_c in order to fit with experimental observations. Subsequently, many other expressions have been proposed to improve this fitting, see [5, Section 10.2.2]. All these corrections lead to modify the infinitesimal thrust dT and consequently the term $a(1-a)$ in Definition (2.19) that becomes:

$$dT = 4\chi(a,a_c)F_\lambda(\varphi)U_{-\infty}^2\rho\pi r dr, \tag{2.21}$$

In the literature, the function $\chi(a,a_c)$ is in most cases of the form:

$$\chi(a,a_c) = a(1-a) + \psi\left((a-a_c)_+\right). \tag{2.22}$$

where $(a-a_c)_+ := \max\{0, a-a_c\}$ and ψ is a given function defined on $\mathbb{R}^+$. Various choices of corrections are presented via the function ψ in Table 2.1. Remark that Glauert's empirical correction leads to a discontinuity at $a = a_c$ as soon as $F_\lambda(\varphi) \neq 1$ (see [5, p.195]). Buhl proposed in [6] a slight modification to fix this issue.

2.4.4. Corrected system. We now repeat the reasoning used to obtain Equations (2.14–2.16), that is, we equalize Equations (2.21) and (2.20) with (2.9) and (2.10) respectively. This gives, using (2.22):

$$\tan\varphi = \frac{1-a}{\lambda(1+a')}, \tag{2.23}$$

$$\frac{a}{1-a} = \frac{1}{\sin^2\varphi}(\mu_L^c(\varphi)\cos\varphi + \mu_D^c(\varphi)\sin\varphi) - \frac{\psi\left((a-a_c)_+\right)}{(1-a)^2}, \tag{2.24}$$

$$\frac{a'}{1-a} = \frac{1}{\lambda\sin^2\varphi}(\mu_L^c(\varphi)\sin\varphi - \mu_D^c(\varphi)\cos\varphi). \tag{2.25}$$

where we have introduced the dimensionless functions

$$\mu_L^c(\varphi) := \frac{\sigma_\lambda}{4F_\lambda(\varphi)}C_L(\varphi-\gamma_\lambda), \quad \mu_D^c(\varphi) := \frac{\sigma_\lambda}{4F_\lambda(\varphi)}C_D(\varphi-\gamma_\lambda), \tag{2.26}$$

defined on I_{β,γ_λ} (see Equation (2.18)) and $\mathbb{R}$, respectively. The corrected model coincides with the simplified model when $F_\lambda(\varphi) = 1$, $a_c = 1$ and $C_D = 0$.

Order	Authors	a_c	$\psi((a-a_c)_+)$
3	Glauert [12]	1/3	$\frac{(a-a_c)_+}{4}\left(\frac{(a-a_c)_+^2}{a_c}+2(a-a_c)_++a_c\right)$
2	Glauert empirical [15, p.25] [22, p.103]	2/5	$a_c(1-a_c)$ $+\frac{(a-a_c)_+[F_\lambda(\varphi)\,((a-a_c)_++2a_c)-0.286]}{2.5708}F_\lambda(\varphi)$
2	Buhl [6]	2/5	$\frac{1}{2F_\lambda(\varphi)}\left(\frac{(a-a_c)_+}{1-a_c}\right)^2$
1	Wilson et al., Spera [30, p.302]	1/3	$(a-a_c)_+^2$

Table 2.1: Various corrections proposed in the literature. The order corresponds to the degree of a in $\chi(a,a_c)$ (see Equations (2.21) and (2.22)) considered as a polynomial with respect to a.

3. Analysis of Glauert's model and existence of solution. In this section, we reduce each of the two previous versions of Glauert's model to a single scalar equation. With a view to obtaining existence results, this leads us to formulate assumptions related to the characteristics of the turbine.

Define the angle $\theta_\lambda \in (0, \frac{\pi}{2})$ by

$$\tan\theta_\lambda := \frac{1}{\lambda}, \tag{3.1}$$

and the intervals

$$\begin{aligned} I :=& I_{\beta,\gamma_\lambda} \cap (-\frac{\pi}{2}+\theta_\lambda, \frac{\pi}{2}+\theta_\lambda), \\ I^+ :=& I \cap (0, \theta_\lambda]. \end{aligned} \tag{3.2}$$

We recall that the set I is non-empty as soon as

$$-\frac{\pi}{2}+\theta_\lambda \leq \beta+\gamma_\lambda. \tag{3.3}$$

3.1. Simplified model. In the setting of the simplified model, a reformulation of Equations (2.14–2.16) can be obtained after a short algebraic manipulation.

THEOREM 3.1. *Suppose that Assumption 1 holds and that* $(\varphi, a, a') \in I - \{0, \frac{\pi}{2}\} \times \mathbb{R} - \{1\} \times \mathbb{R} - \{-1\}$ *satisfies Equations (2.14–2.16). Then* φ *satisfies*

$$\mu_L(\varphi) = \mu_G(\varphi), \tag{3.4}$$

where

$$\mu_G(\varphi) := \sin\varphi \tan(\theta_\lambda - \varphi).$$

Reciprocally, suppose that $\varphi \in I - \{0, \frac{\pi}{2}\}$ *satisfies Equation* (3.4) *and define* a *and* a' *as the corresponding solutions of Equations* (2.15) *and* (2.16)*, respectively. Then* $(\varphi, a, a') \in I - \{0, \frac{\pi}{2}\} \times \mathbb{R} - \{1\} \times \mathbb{R} - \{-1\}$ *satisfies Equations (2.14–2.16).*

Note that Equation (3.4) appears – up to a factor – in [22, p.128], see Equation (3.85a). Some examples of graphs of μ_L and μ_G are given in Section 6.1.

We have excluded the angles $\varphi = \frac{\pi}{2}$ and $\varphi = 0$ for the sole reason that Equations (2.14–2.16) are not defined for these angle values. However, $\varphi = 0$ is naturally associated with the case $a = 1$, as it appears in Equation (2.15). On the other hand, the value $\varphi = \frac{\pi}{2}$, that belongs to I if $\beta + \gamma_\lambda > \frac{\pi}{2} > -\beta + \gamma_\lambda$, is neither a solution of Equations (2.14–2.16) nor of Equation (3.4): setting this value in the former system leads indeed to $a' = -1$, $a = 0$ and $-\lambda = \mu_L(\frac{\pi}{2})$ which corresponds to a negative lift, hence contradicts $C_L \geq 0$ on $I_\beta \cap \mathbb{R}^+$ in Assumption 1. As a matter of fact, these angles can actually be considered when dealing with (3.4), since they do not pose any particular problems concerning the definition of μ_G, and are generally not a solution of this equation. Finally, note that the right-hand side of Equation (3.4) is not defined in the values $\varphi = \pm\frac{\pi}{2} + \theta_\lambda$. However, they do not give rise to any solution of Equations (2.14–2.16): inserting them in the last equations leads to $\mp\lambda = 0.\mu_L(\pm\frac{\pi}{2})$ which contradicts $\lambda = \frac{\Omega r}{U_{-\infty}} > 0$. For all these reasons, the formulation (3.4) will be considered on the whole interval I in the rest of this paper.

Proof. Suppose that $(\varphi, a, a') \in I \times \mathbb{R} - \{1\} \times \mathbb{R} - \{-1\}$ satisfies Equations (2.23–2.25). We have to prove that φ satisfies Equation (3.4). Eliminating a and a' in (2.14) using (2.15) and (2.16), we get:

$$\begin{aligned}\tan^{-1}\varphi = \lambda\frac{1+a'}{1-a} &= \lambda(1+\frac{a}{1-a}) + \lambda\frac{a'}{1-a} \\ &= \lambda\left(1 + \frac{\cos\varphi}{\sin^2\varphi}\mu_L(\varphi)\right) + \frac{1}{\sin\varphi}\mu_L(\varphi).\end{aligned}$$

so that Equation (3.4) follows from the definition (3.1) of θ_λ. Repeating these steps backward ends the proof of the equivalence. ∎

This result shows that Glauert's model – here in its simplified version – essentially boils down to an only scalar equation: indeed, suppose that φ satisfies Equation (3.4), then a and a' can be post-computed thanks to Equations (2.15–2.16). These quantities read as a by-product of the determination of φ.

An important property of Equation (3.4) is that its left-hand side corresponds to the local description of the problem related to Blade Element Theory, whereas its right-hand side is rather related to the macroscopic modeling arising from Momentum Theory. As a consequence, μ_G reads as a universal function of fluid-turbine dynamics depending only on θ_λ, whereas μ_L reads as a function which strictly depends on the turbine under consideration, i.e. on its design parameters γ_λ or σ_λ as well as its 2D experimental data, through C_L. In this view, Equation (3.4) is in line with the approach considered by Glauert. In the same way, the two intervals considered to define I, namely I_{β,γ_λ} and $(-\frac{\pi}{2} + \theta_\lambda, \frac{\pi}{2} + \theta_\lambda)$ play similar roles in the local and in the macroscopic descriptions as they corresponds to the domains of definition of μ_G and μ_L respectively whereas $I_{\beta,\gamma_\lambda} \cap \mathbb{R}^+$ and $(0, \theta_\lambda]$, whose intersection is I^+, correspond to angles associated with positive lift in the two descriptions.

The formulation given in Theorem 3.1 gives rise to many criteria to ensure existence of solution of (3.4): existence indeed holds as soon as the graphs of μ_G and μ_L intersect. As an illustration, we give a simple condition in the case of symmetric profiles. We express the assumptions in terms of μ_L to make it coherent with the formulation (3.4) ; they can however easily be formulated in terms of C_L and σ_λ.

COROLLARY 3.2. *In addition to Assumption 1, suppose that the profile under consideration is symmetric with $\gamma_\lambda > 0$, and that*

$$\mu_G(\max I^+) \leq \mu_L(\max I^+), \tag{3.5}$$

where $\max I^+ := \min\{\theta_\lambda, \beta + \gamma_\lambda\}$, see Equation (3.2). Then Equation (3.4) admits a solution in $[\gamma_\lambda, \max I^+]$ corresponding to a positive lift. Moreover, if $\max I^+ = \theta_\lambda$, i.e. $\theta_\lambda \leq \beta + \gamma_\lambda$, then (3.5) is necessarily satisfied.

Proof. Since $\gamma_\lambda > 0$ and $\beta > 0$, condition (3.3) holds, so that $\max I^+$ is well defined. Recall first that Assumption 1 implies that C_L and consequently μ_L are continuous. As we consider a symmetric profile, we have $\mu_L(\gamma_\lambda) = \frac{\sigma_\lambda}{4} C_L(0) = 0$ whereas $\mu_G(\gamma_\lambda) > 0$. Because of Inequality (3.5), the existence of solution of (3.4) in $[\gamma_\lambda, \max I^+]$ then follows from Intermediate Value Theorem. The positivity of μ_G on the interval $[\gamma_\lambda, \max I^+]$ implies that the resulting lift is positive.

Suppose finally that $\max I^+ = \theta_\lambda$. Assumption 1 guarantees that μ_L is positive on $[\gamma_\lambda, \theta_\lambda]$. Since $\mu_G(\theta_\lambda) = 0$, the last assertion follows. ∎

In the case where μ_L is supplementary assumed to be increasing on $[\gamma_\lambda, \beta + \gamma_\lambda]$, then, the solution defined in Theorem 3.2 is unique.

3.2. Corrected model. We now consider the corrected model defined by Equations (2.23–2.25), for a given value $a_c \in (0, 1)$. The algebraic manipulations performed in the previous section to get Theorem 3.1 cannot be pushed as far as with the simplified model and the resulting expressions still contain the unknown a. Hence, before stating a reformulation of this model and an existence result, we need to clarify the dependence of a on the variable φ. Again, we express our assumptions in terms of μ_L^c and μ_D^c, but the translation in terms of C_L, C_D, σ_λ and $F_\lambda(\varphi)$ is straightforward.

In all this section, we suppose that $0 \in I$, i.e. $|\gamma_\lambda| \leq \beta$, which means in particular that

$$I^+ = (0, \min\{\theta_\lambda, \beta + \gamma_\lambda\}]. \tag{3.6}$$

LEMMA 3.3. *Assume that Assumption 1 holds and define, for $\varphi \in I^+$*

$$g(\varphi) := \tan^{-1}\varphi \tan(\theta_\lambda - \varphi) + \frac{\mu_D^c(\varphi)}{\sin\varphi}\left(1 + \tan^{-1}\varphi \tan(\theta_\lambda - \varphi)\right). \tag{3.7}$$

Let ψ be one of the functions given in Table 2.1, with $F_\lambda(\varphi) = 1$ in the case of Glauert empirical correction. Then, the expression

$$\frac{a}{1-a} + \frac{\sin\theta_\lambda \sin\varphi}{\cos(\theta_\lambda - \varphi)} \frac{\psi\left((a - a_c)_+\right)}{(1-a)^2} = g(\varphi) \tag{3.8}$$

defines a continuous mapping $\tau : \varphi \in I^+ \mapsto a \in [0, 1)$.

Moreover, if g is decreasing and μ_D^c differentiable on I^+, then τ is decreasing and differentiable for all $\varphi \in I^+$ with a possible exception of one point φ_c.

As a by-product of the properties of C_D stated in Assumption 1, the function μ_D^c is always positive and defined for all angles in concrete cases so that g is well defined on I^+. Note also that the only obstruction for g to be decreasing would come from the term C_D which is often increasing in a neighborhood of 0. But for usual profiles, its variations are negligible when compared to the other (decreasing) terms in Equation (3.7).

Proof. For simplicity of notation, let us rewrite Equation (3.8) under the form

$$u(a) + v(\varphi)w(a) = g(\varphi), \tag{3.9}$$

with

$$u(a) := \frac{a}{1-a},\ v(\varphi) := \frac{\sin\theta_\lambda \sin\varphi}{\cos(\theta_\lambda - \varphi)},\ w(a) = \frac{\psi\left((a-a_c)_+\right)}{(1-a)^2}.$$

Let us first consider the left-hand side of Equation (3.9). We see that u is positive and increasing on $[0,1)$ as well as w for any function ψ given in Table 2.1 (with $F_\lambda(\varphi) = 1$ in the case of Glauert empirical correction). In the same way, v is positive and increasing on $(0,\theta_\lambda]$, hence on I^+. Fix now $\varphi \in I^+$, it is fairly easy to see that the mapping $a \in [0,1) \mapsto u(a) + v(\varphi)w(a)$ is continuous, strictly increasing, strictly positive and goes from 0 to $+\infty$. Since g is bounded and assumed to be positive on I^+, there exists an only a in $[0,1)$ such that Equation (3.9) holds. Hence the existence of the mapping τ.

Suppose now that g is decreasing and μ_D^c differentiable. If we set aside the function w in the point $a = a_c$, all the functions involved in Equation (3.9) are differentiable. Consider $\varphi \in I^+$, such that $\tau(\varphi) \neq a_c$. The functions u and w are differentiable in $a = \tau(\varphi) \in (0,1)$ and $u'(a)+v(\varphi)w'(a) \neq 0$ so that we can differentiate Equation (3.9) with respect to φ. We get:

$$\tau'(\varphi) = \frac{g'(\varphi) - v'(\varphi)w\left(\tau(\varphi)\right)}{u'\left(\tau(\varphi)\right) + v(\varphi)w'\left(\tau(\varphi)\right)}.$$

Combining the fact that g is decreasing with the above properties of v, w, u and their derivatives implies that $\tau'(\varphi) \leq 0$. As a consequence, the mapping τ is decreasing and either differentiable on the whole interval I^+, or differentiable on a set of the form $I^+ - \{\varphi_c\}$ where φ_c is the unique value in I^+ such that $\tau(\varphi_c) = a_c$. The result follows. ∎

Remark 3.4. *The quantity $a = \tau(\varphi)$ can generally be computed explicitly provided that the function ψ is specified analytically as, e.g., in Table 2.1. In these cases, the computation consists in solving a low order polynomial equation (in a).*

We can now state a result similar to Theorem 3.1 in the case of the corrected model.

Theorem 3.5. *Let Assumption 1 hold and ψ be one of the functions given in Table 2.1, with $F_\lambda(\varphi) = 1$ in the case of Glauert empirical correction. Suppose also that $(\varphi, a, a') \in I^+ - \{\frac{\pi}{2}\} \times \mathbb{R} - \{1\} \times \mathbb{R}$ satisfies Equations (2.23–2.25). Then φ satisfies*

$$\mu_L^c(\varphi) - \tan(\theta_\lambda - \varphi)\mu_D^c(\varphi) = \mu_G^c(\varphi), \tag{3.10}$$

where

$$\mu_G^c(\varphi) := \mu_G(\varphi) + \frac{\cos\theta_\lambda \sin^2\varphi}{\cos(\theta_\lambda - \varphi)} \frac{\psi\left((\tau(\varphi) - a_c)_+\right)}{(1-\tau(\varphi))^2}. \tag{3.11}$$

Reciprocally, suppose that $\varphi \in I^+ - \{\frac{\pi}{2}\}$ satisfies Equation (3.10) and define a and a' by

$$a = \tau(\varphi), \tag{3.12}$$

$$a' = \frac{1-\tau(\varphi)}{\lambda \sin^2\varphi}(\mu_L^c \sin\varphi - \mu_D^c \cos\varphi). \tag{3.13}$$

Then $(\varphi, a, a') \in I^+ - \{\frac{\pi}{2}\} \times \mathbb{R} - \{1\} \times \mathbb{R}$ satisfies Equations (2.23–2.25).

We refer to Section 6.1 for concrete examples of graphs of μ_G^c, μ_G and $\varphi \mapsto \mu_L^c(\varphi) - \tan(\theta_\lambda - \varphi)\mu_D^c(\varphi)$. As was the case with the simplified model, the value $\varphi = \frac{\pi}{2}$ is excluded only for the technical reason that Equation (2.23) is not defined for this angle.

Proof. Thanks to Lemma 3.3, τ is well defined on I^+. Let $(\varphi, a, a') \in I^+ - \{\frac{\pi}{2}\} \times [0,1) \times \mathbb{R}^+$ satisfying Equations (2.23–2.25). Because of (2.23), we get:

$$\tan^{-1}\varphi = \lambda \frac{1+a'}{1-a} = \lambda(1 + \frac{a}{1-a}) + \lambda \frac{a'}{1-a}.$$

In the previous equation, the terms $\frac{a}{1-a}$ and $\lambda\frac{a'}{1-a}$ can be eliminated thanks to (2.24) and (2.25), respectively. After some algebraic manipulations, we end up with a corrected version of (3.4):

$$\mu_L^c = (\sin\varphi + \mu_D^c)\tan(\theta_\lambda - \varphi) + \frac{\cos\theta_\lambda \sin^2\varphi}{\cos(\theta_\lambda - \varphi)} \frac{\psi\left((a-a_c)_+\right)}{(1-a)^2}, \tag{3.14}$$

so that (3.10) is satisfied. Using (3.14) expression to eliminate μ_L^c in (2.24) gives (3.8). Consequently, Lemma 3.3 implies that a and φ satisfy (3.12). Finally, Equation (3.13) is a direct consequence of (3.12) and (2.25).

Suppose now that $(\varphi, a, a') \in I^+ - \{\frac{\pi}{2}\} \times [0,1) \times \mathbb{R}^+$ satisfies Equations (3.10–3.13). Replacing $\tau(\varphi)$ by a in (3.13) gives immediately Equation (2.25). Combining (3.12) with the definition of μ_G^c give (2.24). Finally, Equation (2.23) is obtained by introducing a and a' into (3.10). ∎

As in the simplified model, Glauert's model boils down to a scalar equation, with φ as an unknown. However, formulation (3.10) does not completely decompose the terms into a local part and macroscopic modeling part: much as the left-hand side of Equation (3.10) still only relies on local features and experimental 2D data of the problem, its right-hand side now also contains an experimental term, namely μ_D^c through the definition of τ.

Before going further, let us give more details about the behavior of τ in $\varphi = 0$.

LEMMA 3.6. *Let Assumption 1 hold and ψ be one of the functions given in Table 2.1, with $F_\lambda(\varphi) = 1$ in the case of Glauert empirical correction.Then*

$$\tau(\varphi) = 1 - \sqrt{\frac{\psi(1-a_c)}{\mu_D^c(0)}}\varphi^{3/2} + o_{\varphi=0}(\varphi^{3/2}).$$

Proof. Thanks to Lemma 3.3, τ is well defined on I^+. Let us first prove that $\lim_{\varphi\to 0^+} \tau(\varphi) = 1^-$. From Equation (3.7), we see that $\lim_{\varphi\to 0^+} g(\varphi) = +\infty$. Given $\varphi \in (0, \theta_\lambda]$, we have $a = \tau(\varphi) \in [0,1)$ and $1 - \frac{\cos\theta_\lambda \cos\varphi}{\cos(\theta_\lambda - \varphi)} = \frac{\sin\theta_\lambda \sin\varphi}{\cos(\theta_\lambda - \varphi)} \geq 0$, so that all the terms of the left-hand side of (3.8) are positive. As a consequence, the only possibility for the sum of these terms to go to $+\infty$ is that $\lim_{\varphi\to 0^+} \tau(\varphi) = 1^-$.

Define now $\nu(\varphi) = 1 - \tau(\varphi)$. We expand (3.8) in a neighborhood $\varphi = 0^+$, which gives:

$$\frac{1}{\nu(\varphi)} - 1 + (\tan\theta_\lambda.\varphi + o_{\varphi=0}(\varphi)) \frac{\psi\left((1-a_c)_+\right) + o_{\varphi=0}(1)}{\nu(\varphi)^2} = \tan\theta_\lambda \frac{\mu_D^c(0)}{\varphi^2} + o_{\varphi=0}(\frac{1}{\varphi^2}),$$

from which we get:

$$\frac{\nu^2(\varphi)}{\varphi^3}\left(\frac{\varphi^2}{\nu(\varphi)} - \varphi^2 - (\tan\theta_\lambda.\mu_D^c(0) + o_{\varphi=0}(1))\right) = -\tan\theta_\lambda \psi\left((1-a_c)_+\right). \tag{3.15}$$

Let $(\varphi_n)_{n\in\mathbb{N}}$ a sequence satisfying $\lim_n \varphi_n = 0^+$, so that $\lim_n \nu(\varphi_n) = 0^+$. Suppose that $\lim_n \frac{\nu^2(\varphi_n)}{\varphi_n^3} = +\infty$. Since $\frac{\varphi_n^2}{\nu(\varphi_n)} = \left(\frac{\varphi_n^3}{\nu^2(\varphi_n)}\right)^{2/3} \nu^{1/3}(\varphi_n)$ this sequence goes to zero. Back to (3.15), we find a contradiction since the left-hand side goes to $+\infty$ whereas the right-hand side is constant. It follows that, up to a subsequence, we can assume that $\lim_n \frac{\nu^2(\varphi_n)}{\varphi_n^3} = \ell$ for a certain ℓ. Setting $\varphi = \varphi_n$ in (3.15) and passing to the limit $n \to +\infty$, we obtain that $\ell = \frac{\psi((1-a_c)_+)}{\mu_D^c(0)}$. The result follows. ∎

Remark 3.7. *In the case $\mu_D^c(0) = 0$, a similar reasoning gives:*

$$\tau(\varphi) = 1 - \sqrt{\psi(1-a_c)\varphi} + o_{\varphi=0}(\varphi^{1/2}).$$

The quantity $\mu_D^c(0) = \frac{\sigma_\lambda}{4} C_D(-\gamma_\lambda)$ has no specific physical meaning in the applications. We have introduced it as a constant (that can be expressed explicitly), for simplicity of presentation. As a matter of fact, the angle $\varphi = 0$ has rather a meaning from the macroscopic point of view, as appears when considering μ_G (that cancels in 0) and μ_G^c, see Equation (3.17) hereafter.

We are now in a position to give an existence result about the corrected model.

Corollary 3.8 (of Theorem 3.5). *Suppose that Assumption 1 holds and that*

$$\mu_G^c(\max I^+) \le \mu_L^c(\max I^+) - \tan(\theta_\lambda - \max I^+)\mu_D^c(\max I^+). \tag{3.16}$$

Then Equation (3.10) admits a solution in I^+ corresponding to a positive lift. Moreover if g is decreasing, $\max I^+ = \theta_\lambda$ and $\varphi^c < \theta_\lambda$, where φ^c is defined in Lemma 3.3, then (3.16) is necessarily satisfied.

Proof. Because of Lemma 3.6 and Definition (3.11) of μ_G^c, we get

$$\mu_G^c(\varphi) \approx_{\varphi\to 0^+} \frac{\mu_D^c(0)}{\varphi},$$

so that

$$\lim_{\varphi\to 0^+} \mu_G^c(\varphi) = +\infty. \tag{3.17}$$

This implies that there exists a small enough $\varphi_0 > 0$ such that $\mu_G^c(\varphi_0) \ge \mu_L^c(\varphi_0) - \tan(\theta_\lambda - \varphi_0)\mu_D^c(\varphi_0)$. Because of the assumption (3.16), the existence of a solution of Equation (3.10) then follows from Intermediate Value Theorem. The positivity of μ_G^c on I^+ implies that the resulting lift is positive.

Suppose now that g is decreasing, $\max I^+ = \theta_\lambda$ and $\varphi^c < \theta_\lambda$. Because of the last assertion of Lemma 3.6, τ is decreasing and the correction associated with ψ is not any more active on $[\varphi^c, \theta_\lambda)$. We then have:

$$\begin{aligned}\mu_G^c(\max I^+) &= \mu_G(\max I^+) = \mu_G(\theta_\lambda)\\ &\le 0 \le \mu_L^c(\max I^+) = \mu_L^c(\max I^+) - \tan(\theta_\lambda - \max I^+)\mu_D^c(\max I^+).\end{aligned}$$

As a consequence, Equation (3.16) is satisfied. ∎

Unlike the simplified model, no condition on γ_λ or $\mu_L^c(\gamma_\lambda)$ is assumed to get the previous result, but the alternative assumption (3.6) is required. This makes the corrected model much better posed than its simplified version.

REMARK 3.9. *In the case $\mu_D^c(0) = 0$, a similar reasoning gives:*

$$\mu_G^c(\varphi) \approx_{\varphi \to 0^+} (1 + \tan\theta_\lambda)\varphi.$$

As a consequence, $\mu_G^c(0) = 0$, so that, as in the simplified model, one needs an assumption about, e.g., $\mu_L^c(\gamma_\lambda)$ to get an existence result similar to Corollary 3.2.

3.3. Multiple solutions. The results of the previous sections can be completed by some additional remarks about cases of non unique solution. Our two versions of Glauert's model may have indeed multiple solutions, that can be sorted into three independent categories:

1. Multiple solutions in the simplified model: since $\lim_{\varphi \to \theta_\lambda \pm \pi/2} \mu_G(\varphi) = -\infty$, there shall be two intersections between the graphs of μ_G and μ_L, e.g. in the case where μ_L is affine on a large enough interval, $C_L(0) = 0$ and $\gamma_\lambda \in (0, \theta_\lambda]$. In this case, one of the two roots gives rise to a negative lift.
2. Multiple solutions caused by stall: as mentioned in Section 2.1.2, the stall phenomenon is generally associated with a sudden decrease in C_L. It follows that if the stall angle α_s satisfies $\alpha_s + \gamma_\lambda \in I$, the graph of μ_L shall cross the graph of μ_G at an angle in $\varphi \geq \alpha_s + \gamma_\lambda$. This fact is reported in [22, p.129]: *"In the stall region [...] there may be multiple solutions for C_L. Each of these solutions is possible. The correct solution should be that which maintains the continuity of the angle of attack along the blade span."*
3. Multiple solutions in the corrected model: though $\lim_{\varphi \to 0^+} \mu_G^c(\varphi) = +\infty$, the graph of μ_G^c may no longer be concave on I^+ when a correction is used for values of a close to 1. Hence possible multiple solutions, e.g. in the case μ_L is affine.

Practical cases where these types of multiple solutions are observed in practice, see Section 6.

4. Solution algorithms. To solve numerically Glauert's model, a specific fixed-point solution algorithm is often highlighted in the litterature. In this section, we recall its main features and introduce more efficient procedures.

4.1. The usual algorithm. Solving the simplified or the corrected model is usually done by a dedicated fixed-point procedure, see [5, 14, 22, 28, 29] or the early presentation in [32, p.47]. This algorithm consists in repeating iteratively the sequen-

Algorithm 4.1 Solving BEM system, usual procedure

Input: Tol > 0, $\alpha \mapsto C_L(\alpha)$, $\alpha \mapsto C_D(\alpha)$, λ, γ_λ, σ_λ, F_λ, $x \mapsto \psi(x)$.
Initial guess: a, a'.
Output: a, a', φ.
Set $err :=$ Tol $+ 1$.
Define the functions μ_L^c and μ_D^c by (2.26) using the input data.
while $err >$ Tol **do**
  Set $\varphi := \text{atan}\left(\frac{1-a}{\lambda(1+a')}\right)$.
  Set a as the solution of (2.24).
  Set $a' = \frac{1-a}{\lambda \sin^2\varphi}(\mu_L^c \sin\varphi - \mu_D^c \cos\varphi)$.
  Set $err := \left|\tan\varphi - \frac{1-a}{\lambda(1+a')}\right|$.
end while

tial solving of Equation (2.23), then Equation (2.24) and finally Equation (2.25). The stopping criterion we have used is arbitrary and usually not mentioned in monographs.

The convergence of this algorithm is problematic. Instabilities are often observed in practice, as reported, e.g., in [28] :

"Note that this set of equations must be solved simultaneously, and in practice, numerical instability can occur." "When local angle of attack is around the stall point, or becomes negative, getting the BEM code to converge can become difficult."

We also refer to [21] for a specific study of some convergence issues. The analysis of the algorithm is tedious ; we refer to Appendix for an example of setting where the convergence is guaranteed.

4.2. Alternative algorithms. Thanks to our new formulation, we can propose some alternative strategies and systematic approaches to compute a solution of the corrected model.

4.2.1. A fixed-point procedure associated with (3.10). In view of Equation (3.10), we consider now an alternative fixed-point procedure based on the iteration

$$\varphi^{k+1} = f(\varphi^k), \tag{4.1}$$

with

$$f(\varphi) = \varphi + \rho(\varphi)\left(\mu_G^c(\varphi) - \mu_L^c(\varphi) + \tan(\theta_\lambda - \varphi)\mu_D^c(\varphi)\right) \tag{4.2}$$

where $\rho(\varphi)$ is a given positive coefficient. The procedure is summarized in Algorithm 4.2.

Algorithm 4.2 Solving BEM system, new fixed-point procedure

Input: Tol > 0, $\alpha \mapsto C_L(\alpha)$, $\alpha \mapsto C_D(\alpha)$, λ, γ_λ, σ_λ, F_λ, $x \mapsto \psi(x)$.
Initial guess: φ.
Output: φ.
Set $err := \text{Tol} + 1$.
Define the functions μ_L^c and μ_D^c by (2.26) using the input data, and f by (4.2).
while $err >$ Tol **do**
  Compute $a := \tau(\varphi)$, i.e. the solution of Equation (3.8).
  Compute $\mu_G^c(\varphi)$, using (3.11).
  Set $err := |f(\varphi) - \varphi|$.
  Set $\varphi = f(\varphi)$.
end while

We then have the following result of convergence in the case $\psi = 0$.

THEOREM 4.1. *Suppose that* $\max I^+ = \theta_\lambda$, $\psi = 0$, *and that Assumption 1 holds. Assume also that* μ_L^c *and* μ_D^c *are continuously differentiable on* I^+, *with* μ_L^c *and* μ_D^c *non-decreasing. If Equations (2.14–2.16) admit at least one solution in* I^+, *then the sequence* $(\varphi^k)_{k\in\mathbb{N}}$ *defined by Equation (4.1) with*

$$\rho(\varphi) = \rho_\varepsilon(\varphi) := \frac{\varepsilon}{\max\{0, -\mu_G'(\varphi)\} + \max_{I^+} \mu_L^{c\,\prime} + \left(1 + \tan^2\theta_\lambda\right)\mu_D^c(\varphi)}, \tag{4.3}$$

for an arbitrary $\varepsilon \in (0,1)$ *and the initial value*

$$\varphi^0 = \theta_\lambda \tag{4.4}$$

converges to $\varphi^\star$, the largest solution of (3.10) in $(0,\theta_\lambda]$.

Proof. The assumptions on μ_L^c and μ_D^c guarantee that the denominator in (4.3) does not cancel so that $\rho_\varepsilon(\varphi)$ is well-defined and positive. We first prove that f is increasing on $[\varphi^\star,\theta_\lambda]$. Since $\varphi\mapsto\rho_\varepsilon(\varphi)$ is decreasing on I^+ and because $\mu_G^c(\varphi)-\mu_L^c(\varphi)+\tan(\theta_\lambda-\varphi)\mu_D^c(\varphi)$ is negative on $[\varphi^\star,\theta_\lambda]$, we have:

$$\begin{aligned}
f'(\varphi) =& 1+\rho_\varepsilon(\varphi)\left(\mu_G'(\varphi)-\mu_L^c{}'(\varphi)-(1+\tan^2(\theta_\lambda-\varphi))\mu_D^c(\varphi)+\tan(\theta_\lambda-\varphi)\mu_D^c{}'(\varphi)\right)\\
&+\rho_\varepsilon{}'(\varphi)\left(\mu_G(\varphi)-\mu_L^c(\varphi)+\tan(\theta_\lambda-\varphi)\mu_D^c(\varphi)\right)\\
\geq& 1-\rho_\varepsilon(\varphi)\left(\max\{0,-\mu_G'(\varphi)\}+\max_{I^+}\mu_L^c{}'+\left(1+\tan^2\theta_\lambda\right)\mu_D^c(\varphi)\right)\\
=& 1-\varepsilon\geq 0.
\end{aligned}$$

Let us then show that $[\varphi^\star,\theta_\lambda]$ is stable by f. Since f is increasing and $f(\varphi^\star)=\varphi^\star$, it remains to show that $f(\theta_\lambda)\leq\theta_\lambda$. This property follows from:

$$\begin{aligned}
f(\theta_\lambda) &= \theta_\lambda+\rho_\varepsilon(\theta_\lambda)\left(\mu_G(\theta_\lambda)-\mu_L^c(\theta_\lambda)\right)\\
&= \theta_\lambda-\rho_\varepsilon(\theta_\lambda)\mu_L^c(\theta_\lambda)\leq\theta_\lambda,
\end{aligned}$$

where we have used that μ_L^c is non-decreasing.
Since $\varphi^0=\theta_\lambda$, $(\varphi^k)_{k\in\mathbb{N}}$ is bounded, monotonically decreasing, hence converges. The result follows from the definition of $\varphi^\star$. ∎

The efficiency of Algorithm 4.2 on the value assigned to ρ. In some cases, we can estimate the rate of convergence of $(\varphi^k)_{k\in\mathbb{N}}$, as stated in the next result.

THEOREM 4.2. *In addition to the assumptions of Theorem 4.1, suppose that*

$$\tan\theta_\lambda(1+\max_{I^+}\mu_D^c{}')<\min_{I^+}\mu_L^c{}'. \tag{4.5}$$

Then the sequence $(\varphi^k)_{k\in\mathbb{N}}$ defined by (4.1–4.4) satisfies

$$|\varphi^k-\varphi^\star|\leq\left(1-\frac{\min_{I^+}\mu_L^c{}'-\tan\theta_\lambda(1+\max_{I^+}\mu_D^c{}')}{\max_{I^+}\mu_L^c{}'+\sin\theta_\lambda+(1+\tan^2\theta_\lambda)\mu_D^c(\theta_\lambda)}\right)^k|\theta_\lambda-\rho_\varepsilon(\theta_\lambda)\mu_L^c(\theta_\lambda)|.$$

Proof. For we have already shown in the previous proof that $f'(\varphi)\geq 0$ on $[\varphi^\star,\theta_\lambda]$, it remains to determine an upper bound for $f'(\varphi)$. To do this, we use the bound (4.5) and $\mu_G'(\varphi)\leq\mu_G'(0)=\tan\theta_\lambda$ to get:

$$\begin{aligned}
f'(\varphi) &= 1+\rho_\varepsilon\left(\mu_G'(\varphi)-\mu_L^c{}'(\varphi)-(1+\tan^2(\theta_\lambda-\varphi))\mu_D^c(\varphi)+\tan(\theta_\lambda-\varphi)\mu_D^c{}'(\varphi)\right)\\
&\leq 1-\rho_\varepsilon\left(\min_{I^+}\mu_L^c{}'-\tan\theta_\lambda(1+\max_{I^+}\mu_D^c{}')\right)\\
&\leq 1-\frac{\min_{I^+}\mu_L^c{}'-\tan\theta_\lambda(1+\max_{I^+}\mu_D^c{}')}{\max_{I^+}\mu_L^c{}'+\sin\theta_\lambda+(1+\tan^2\theta_\lambda)\mu_D^c(\theta_\lambda)},
\end{aligned}$$

where we have used $\max\{0,-\mu_G'(\varphi)\}\geq-\mu_G'(\theta_\lambda)=\sin\theta_\lambda$ to bound ρ_ε from below. The result in then obtained by induction. ∎

One can actually obtain quadratic convergence, i.e. $|\varphi^k-\varphi^\star|\leq\delta|\varphi^0-\varphi^\star|^{2^k}$ for some $\delta>0$ by using a Newton procedure, that is, by replacing $\rho(\varphi)$ in (4.3) by the

sequence $(\rho^k)_{k\in\mathbb{N}}$ defined by

$$\rho^k := -\frac{1}{\mu_G'(\varphi^k) - \mu_L^c{}'(\varphi^k) - (1+\tan^2(\theta_\lambda-\varphi^k))\mu_D^c(\varphi^k) + \tan(\theta_\lambda-\varphi^k)\mu_D^c{}'(\varphi^k)}.$$

and by choosing φ^0 close enough to $\varphi^\star$. Though the term $\mu_G'(\varphi^k)$ can be computed exactly as well as most of the terms in the denominator, the previous expression remains difficult to evaluate since the functions μ_L^c and μ_D^c are only known experimentally, i.e. pointwise, hence require an interpolation procedure.

4.2.2. The general case. If a correction for high values of a is considered and applies, then the framework of Corollary 3.8 implies that there exists a solution of the corrected model in I^+. In this case, a bisection algorithm applied to Equation (3.10) converges to a solution. This procedure is given in Algorithm 4.3.

Algorithm 4.3 Solving BEM system, bisection algorithm

Input: Tol >0, $\alpha\mapsto C_L(\alpha)$, $\alpha\mapsto C_D(\alpha)$, λ, γ_λ, σ_λ, F_λ, $x\mapsto\psi(x)$.
Initial guess: φ^+, φ^- with $\varphi^+>\varphi^-$.
Output: φ.
Set $err :=$ Tol $+1$.
Define the functions μ_L^c and μ_D^c by (2.26) using the input data, and

$$b(\varphi) := \mu_G^c(\varphi) - \mu_L^c(\varphi) + \tan(\theta_\lambda-\varphi)\mu_D^c(\varphi).$$

if $b(\varphi^+)b(\varphi^-)>0$ **then**
  Abort *//wrong initial guess*
end if
while $err >$ Tol **do**
  Compute $a := \tau(\frac{\varphi^++\varphi^-}{2})$, i.e. the solution of Equation (3.8)
  Compute $b(\frac{\varphi^++\varphi^-}{2})$, using (3.11)
  if $b(\varphi^+)b(\frac{\varphi^++\varphi^-}{2})>0$, **then**
    Set $\varphi^+ = \dfrac{\varphi^++\varphi^-}{2}$
    Set $\varphi^- = \frac{\varphi^++\varphi^-}{2}$.
  end if
  Set $err := |\varphi^+-\varphi^-|$.
end while

As was the case with the others procedures, such an algorithm requires to solve at each iteration an implicit equation, namely $a=\tau(\varphi)$, i.e. Equation (3.8) that has been discussed in Remark 3.4.

We finally show that the solution found in the case $\psi=0$ can be used to bracket the solution in the general case of the corrected model.

LEMMA 4.3. *Keep the assumptions of Corollary 3.8, and denote by φ_0 a solution Equation (3.10) where $\psi=0$. Then Equation (3.10) admits a solution in $(\varphi_0, \min\{\theta_\lambda, \beta+\gamma_\lambda\}]$ corresponding to a positive lift.*

Proof. Since φ_0 satisfies Equation (3.10) with $\psi=0$, we have:

$$\mu_L^c(\varphi_0) - \tan(\theta_\lambda-\varphi_0)\mu_D^c(\varphi_0) - \mu_G^c(\varphi_0) = -\frac{\cos\theta_\lambda \sin^2\varphi_0}{\cos(\theta_\lambda-\varphi_0)}\frac{\psi\left((\tau(\varphi_0)-a_c)_+\right)}{(1-\tau(\varphi_0))^2} \le 0.$$

We then use (3.16) and Intermediate Value Theorem to conclude. ∎

5. Optimization. The BEM model does not only aim to evaluate the efficiency of a given geometry, but also provides a method to design rotors, that is, to select high-performance parameters γ_λ and c_λ. In this way, monographs generally consider maximization procedures of a particular functional C_p, often called *power coefficient* ([22, p.129, Equation (3.90a)], [12, p.328]), which corresponds to the ratio between the received and the captured energy. This quantity is defined by

$$C_p(\gamma_\lambda, c_\lambda, \varphi, a, a') = \frac{8}{\lambda_{\max}^2} \int_{\lambda_{\min}}^{\lambda_{\max}} \lambda^3 J_\lambda(\gamma_\lambda, c_\lambda, \varphi, a, a') d\lambda,$$

with

$$J_\lambda(\gamma_\lambda, c_\lambda, \varphi, a, a') := F_\lambda(\varphi) a'(1-a) \left(1 - \frac{C_D(\varphi - \gamma_\lambda)}{C_L(\varphi - \gamma_\lambda)} \tan^{-1} \varphi\right), \tag{5.1}$$

and under the constraints (2.23–2.25). The drag coefficient C_D is consequently taken into account (though partly neglected in the reasoning, as explained hereafter) as well as the Tip loss correction. As far as we know, no corrections related to high values of a, such as those presented in Section 2.4.3, are considered in optimization procedures. This motivates the description of an optimization algorithm for the corrected model that we give in Section 5.2.

5.1. Simplified model and usual optimum approximation. The usual optimization procedure is described in, e.g., [22, p.131-137]. For the sake of completeness, we recall it in the case where $F_\lambda = 1$.

Considering independently each λ on a discretization grid associated with the interval $[\lambda_{\min}, \lambda_{\max}]$ and the corresponding functional $J_\lambda(\gamma_\lambda, c_\lambda, \varphi, a, a')$, the first step consists in defining an angle $\overline{\alpha}$ which minimizes the ratio $\frac{C_D(\alpha)}{C_L(\alpha)}$. In the following steps, the coefficient C_D is simply neglected: not only the factor $1 - \frac{C_D(\varphi-\gamma_\lambda)}{C_L(\varphi-\gamma_\lambda)} \tan^{-1}(\varphi)$ is set to 1 in (5.1), but C_D is also set to 0 in the constraints, which then correspond to the simplified model (2.14–2.16). Then, Theorem 3.1 allows us to replace μ_L by μ_G in Equations (2.15–2.16) so that a, a', and consequently J_λ can be expressed exclusively in terms of φ, namely

$$a = 1 - \frac{\sin\varphi\cos(\theta_\lambda - \varphi)}{\sin\theta_\lambda},\ a' = \frac{\sin\varphi\sin(\theta_\lambda - \varphi)}{\cos\theta_\lambda},\ J_\lambda = \frac{\sin^2\varphi\sin\left(2(\theta_\lambda - \varphi)\right)}{\sin 2\theta_\lambda}.$$

It remains to optimize $\varphi \mapsto \sin^2\varphi\sin(2(\theta_\lambda - \varphi))$, for $\varphi \in [0, \theta_\lambda]$. An easy computation shows that the maximum is attained at $\varphi^* = \frac{2}{3}\theta_\lambda$. Finally, the design parameters $\gamma_\lambda^* = \gamma_\lambda(\varphi^*)$ and $c_\lambda^* = c_\lambda(\varphi^*)$ can then be computed from Equations (2.5) and (3.4), to get

$$\gamma_\lambda^* = \varphi^* - \overline{\alpha},\ \ c_\lambda^* = \frac{8\pi r \mu_G(\varphi^*)}{B C_L(\overline{\alpha})}. \tag{5.2}$$

5.2. A gradient method for the corrected model. We now detail an adjoint-based gradient method than can be used to tackle the optimization of γ_λ and c_λ in the framework of the corrected model. Since the elements are also independent in the corrected model, we still consider the optimization problem associated with an element, i.e., we fix the value of λ and optimize J_λ. Throughout this section, we denote

by C_L' and C_D' the derivatives of C_L and C_D respectively, and omit in notation the dependence of μ_L and μ_D and their derivatives on the variable φ.

We first recall how the introduction of Lagrange multipliers enables to compute the gradient of J_λ. Define the Lagrangian of Problem (5.1) by

$$\begin{aligned}
&\mathcal{L}_\lambda(\varphi, a, a', p_1, p_2, p_3, c_\lambda, \gamma_\lambda) \\
&\qquad := J_\lambda(\varphi, a, a', c_\lambda, \gamma_\lambda) - p_1\left(\mu_L(\varphi) - \tan(\theta_\lambda - \varphi)\mu_D(\varphi) - \mu_G^c(\varphi)\right) \\
&\qquad\quad - p_2\left(\frac{a}{1-a} - \frac{1}{\sin^2\varphi}(\mu_L^c(\varphi)\cos\varphi + \mu_D^c(\varphi)\sin\varphi) + \frac{\psi\left((a-a_c)_+\right)}{(1-a)^2}\right) \\
&\qquad\quad - p_3\left(\frac{a'}{1-a} - \frac{1}{\lambda\sin^2\varphi}(\mu_L^c(\varphi)\sin\varphi - \mu_D^c(\varphi)\cos\varphi\right),
\end{aligned}$$

where p_1, p_2 and p_3 are the Lagrange multipliers associated with the constraints (2.23–2.25). The optimality system is obtained by canceling all the partial derivatives of $\mathcal{L}_\lambda$. Differentiating $\mathcal{L}_\lambda$ with respect to p_1, p_2 and p_3 and equating the resulting terms to zero gives the corrected model Equations (2.23–2.25), that can be solved using the algorithms presented in Section 4. Setting the derivatives of $\mathcal{L}_\lambda$ with respect to (φ, a, a') to zero gives rise to the linear system

$$M \cdot p = b \tag{5.3}$$

where $p := (p_1 \;\; p_2 \;\; p_3)^\top$ is the Lagrange multiplier vector, and

$$\begin{aligned}
M &:= \begin{bmatrix}
\frac{1}{\cos^2\varphi} & \frac{\mu_D - \frac{\partial\mu_L}{\partial\varphi}}{\sin\varphi\tan\varphi} + \frac{\mu_L(1-2\tan^{-2}\varphi) - \frac{\partial\mu_D}{\partial\varphi}}{\sin\varphi} & \frac{\mu_L + \frac{\partial\mu_D}{\partial\varphi}}{\lambda\sin\varphi\tan\varphi} - \frac{\frac{\partial\mu_L}{\partial\varphi} + \mu_D(1+2\tan^{-2}\varphi)}{\lambda\sin\varphi} \\
-\frac{1}{\lambda(1+a')} & \frac{1+\psi'((a-a_c)_+)}{(1-a)^2} + \frac{2\psi((a-a_c)_+)}{(1-a)^3} & \frac{a'}{(1-a)^2} \\
\frac{1-a}{\lambda(1+a')^2} & 0 & \frac{1}{1-a}
\end{bmatrix} \\
b &:= \frac{8F_\lambda(\varphi)\lambda^3}{\lambda_{max}^2}\begin{pmatrix}
a'(1-a)\frac{C_L'(\varphi-\gamma_\lambda)C_D(\varphi-\gamma_\lambda) - C_D'(\varphi-\gamma_\lambda)C_L(\varphi-\gamma_\lambda)}{C_L(\varphi-\gamma_\lambda)^2\tan\varphi} + \frac{C_D(\varphi-\gamma_\lambda)}{C_L(\varphi-\gamma_\lambda)\sin^2\varphi} \\
-a'\frac{1-C_D(\varphi-\gamma_\lambda)}{C_L(\varphi-\gamma_\lambda)\tan\varphi} \\
(1-a)\frac{1-C_D(\varphi-\gamma_\lambda)}{C_L(\varphi-\gamma)\tan\varphi}
\end{pmatrix} \\
&\quad + \frac{8F_\lambda'(\varphi)\lambda^3}{\lambda_{max}^2}\begin{pmatrix}
a'(1-a)\frac{1-C_D(\varphi-\gamma_\lambda)}{C_L(\varphi-\gamma_\lambda)\tan\varphi} \\
0 \\
0
\end{pmatrix}.
\end{aligned}$$

We are now in a position to detail how the gradient can be computed and included in an optimization procedure. Fix the values of the pair $(\gamma_\lambda, c_\lambda)$. If φ, a, a' are the corresponding solutions of Equations (2.23–2.25) and p is the associated solution of Equation (5.3), then the gradient $\nabla J_\lambda(\gamma_\lambda, c_\lambda)$ of $J_\lambda(\gamma_\lambda, c_\lambda)$ is given by

$$\nabla J_\lambda(\gamma_\lambda, c_\lambda) = \begin{pmatrix} \frac{\partial\mathcal{L}_\lambda}{\partial\gamma_\lambda} & \frac{\partial\mathcal{L}_\lambda}{\partial c_\lambda} \end{pmatrix}^\top, \tag{5.4}$$

where

$$\frac{\partial \mathcal{L}_\lambda}{\partial \gamma_\lambda} = a'(1-a)\frac{C_D'(\varphi-\gamma_\lambda)C_L(\varphi-\gamma_\lambda) - C_L'(\varphi-\gamma_\lambda)C_D(\varphi-\gamma_\lambda)}{C_L^2(\varphi-\gamma_\lambda)\tan\varphi}$$
$$- p_2\frac{1}{\sin^2\varphi}\left(\frac{\partial \mu_L}{\partial \varphi}\cos\varphi + \frac{\partial \mu_D}{\partial \varphi}\sin\varphi\right) - p_3\frac{1}{\lambda\sin^2\varphi}\left(\frac{\partial \mu_L}{\partial \varphi}\sin\varphi - \frac{\partial \mu_D}{\partial \varphi}\cos\varphi\right),$$
$$\frac{\partial \mathcal{L}_\lambda}{\partial c_\lambda} = p_2\frac{1}{\sin^2\varphi}\left(\frac{\partial \mu_L}{\partial c_\lambda}\cos\varphi + \frac{\partial \mu_D}{\partial c_\lambda}\sin\varphi\right) + p_3\frac{1}{\lambda\sin^2\varphi}\left(\frac{\partial \mu_L}{\partial c_\lambda}\sin\varphi - \frac{\partial \mu_D}{\partial c_\lambda}\cos\varphi\right).$$

The associated optimization procedure is then formalized with Algorithm 5.1.

Algorithm 5.1 Numerical optimization

Input: Tol > 0, $\kappa > 0$, $\alpha \mapsto C_L(\alpha)$, $\alpha \mapsto C_D(\alpha)$, λ, $x \mapsto \psi(x)$.
Initial guess: $\gamma_\lambda, c_\lambda$.
Output: $\gamma_\lambda, c_\lambda$.
Set $err := \text{Tol} + 1$.
Define the functions μ_L^c and μ_D^c by (2.26) using the input data.
while $err >$ Tol **do**
  Set φ, a, a' as the solutions of Equations (2.23–2.25).
  Set p as the solution of Equation (5.3).
  Compute the gradient $\nabla J_\lambda(\gamma_\lambda, c_\lambda)$ given by Equation (5.4).
  Update $\begin{pmatrix} c_\lambda \\ \gamma_\lambda \end{pmatrix} = \begin{pmatrix} c_\lambda \\ \gamma_\lambda \end{pmatrix} + \kappa \nabla J_\lambda(\gamma_\lambda, c_\lambda)$,
  Set $err := \|\nabla J_\lambda(\gamma_\lambda, c_\lambda)\|$.
end while

6. Numerical experiments. In this section, we investigate the performance of the algorithms presented in Section 4 on a practical case and study numerically the design optimization problem considered in Section 5.

6.1. Case study. We consider a turbine of radius $R = 1.1$m, consisting of three blades, designed with a NACA 4415 profile. The associated functions C_L and C_D have been obtained using truncated Fourier representations of data provided by the free software Xfoil [8]. The first step of the usual design procedure presented in Section 5.1 gives in this case $\overline{\alpha} = 0.2215$ rad. Plots of C_L and C_D are given in Figure 6.1.

We use the correction from Wilson *et al* and Spera, meaning that $a_c = 1/3$, see Table 2.1. We first focus on three different blade elements associated with $\lambda_1 = 0.5$, $\lambda_2 = 1.75$, and $\lambda_3 = 3$, respectively. In these three cases, we either set $(\gamma_\lambda, c_\lambda) = (\gamma_\lambda^*, c_\lambda^*)$, i.e. we use the optimal values of the simplified model given by (5.2) or the values obtained via Algorithm 5.1, i.e. we use optimal values $(\gamma_\lambda, c_\lambda) =: (\gamma_\lambda^c, c_\lambda^c)$ associated with the corrected model. These values, as well as the associated values of φ_c are given in Table 6.1, whereas corresponding graphs of the functions $\mu_{LD}^c : \varphi \mapsto \mu_L^c(\varphi) - \tan(\theta_\lambda - \varphi)\mu_D^c(\varphi)$, μ_G^c and μ_G are presented in Figure 6.2.

For these two blade geometries, $I^+ = (0, \theta_\lambda]$, $\varphi^c < \theta_\lambda$ for all elements (see Definition (3.6)). However, the function g is non-decreasing in few cases, as, e.g. when $\lambda = 0.5$ and $(\gamma_\lambda, c_\lambda) = (\gamma_\lambda^*, c_\lambda^*)$. In this case, the last statement of Lemma 3.3 about the uniqueness of φ_c does not apply which explains the existence of two values φ_c^1 and φ_c^2 where the graphs of μ_G^c and μ_G merge or separate. In the other examples, Corollary 3.8 applies, which is confirmed by the plots.

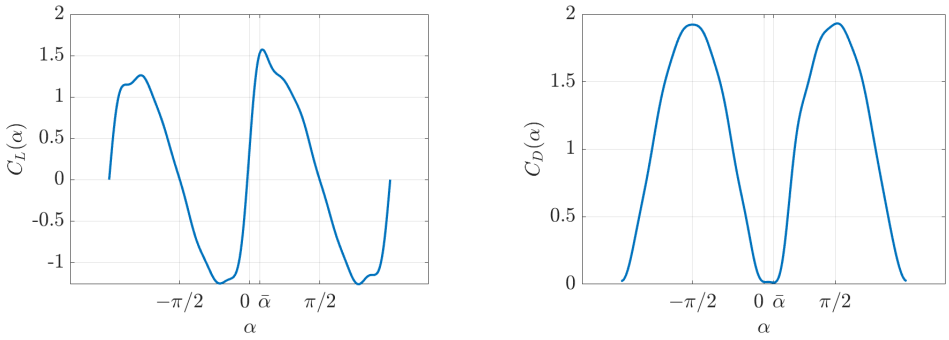

Figure 6.1: Lift and Drag coefficients C_L and C_D as functions of the angle of attack α.

λ	γ_λ^*	γ_λ^c	c_λ^*	c_λ^c	$\varphi_c \quad (\gamma_\lambda^*, c_\lambda^*)$	$\varphi_c \quad (\gamma_\lambda^c, c_\lambda^c)$
$\lambda_1 = 0.5$	0.516627	0.520195	1.429701	0.255311	(0.715856,0.996060)	0.707018
$\lambda_2 = 1.75$	0.124625	0.123680	0.318397	0.200768	0.343358	0.343095
$\lambda_3 = 3$	-0.006972	-0.052160	0.045246	0.066050	0.213839	0.214025

Table 6.1: Optimal values of the twist γ_λ and the chord c_λ for various values of λ, with $(\gamma_\lambda, c_\lambda) = (\gamma_\lambda^*, c_\lambda^*)$ and $(\gamma_\lambda, c_\lambda) =: (\gamma_\lambda^c, c_\lambda^c)$.

We observe that multiple solutions of type (1) (see Section 3.3) may occur in the case of the simplified model. On the other hand, the corrected model always gives rise to a unique solution. The performances obtained with $(\gamma_\lambda^*, c_\lambda^*)$ and $(\gamma_\lambda^c, c_\lambda^c)$ are compared in Section 6.3.

6.2. Solution algorithms. In this section, we compare the various solution algorithms in terms of number of iterations. More precisely, we measure the number k of iterations required to solve accurately (3.10) in the sense that

$$err := \left|\mu_L^c(\varphi^k) - \tan(\theta_\lambda - \varphi^k)\mu_D^c(\varphi^k) - \mu_G^c(\varphi^k)\right| \leq \text{Tol} = 10^{-10}, \tag{6.1}$$

meaning that we consider the corrected model. We test the three algorithms presented in Section 4, namely, the usual procedure described in Algorithm 4.1, the new fixed-point procedure described in Algorithm 4.2 and the bisection algorithm detailed in Algorithm 4.3. For Algorithm 4.1, we set $\rho = \rho_1$, i.e. the value given by Equation (4.3) (though we include in our test a correction on a), with $\varepsilon = 1$. To get a fair comparison, we use (6.1) to define the stopping criterion in all our tests, instead of the respective definitions of err given in the algorithms. Remark that due to the choice of Wilson *et al* and Spera's correction, iterations in three algorithms have similar computational cost, namely, the solving second order polynomials corresponding to Equation (2.24) or (3.8) as required in Algorithm 4.1 or in Algorithms 4.2 and 4.3, respectively.

The initialization is done with $\varphi^0 = \theta_\lambda$ for Algorithm 4.1 and Algorithm 4.2, whereas Algorithm 4.3 is initialized with the interval $I_0 := [\varphi^-, \varphi^+] = [10^{-4}, \theta_\lambda]$. The blade under consideration is the one described in the previous section, with $\gamma_\lambda = \gamma_\lambda^*$ and $c_\lambda = c_\lambda^*$. We run our test on the two cases $a_c = 1$ and $a_c = 1/3$. The former

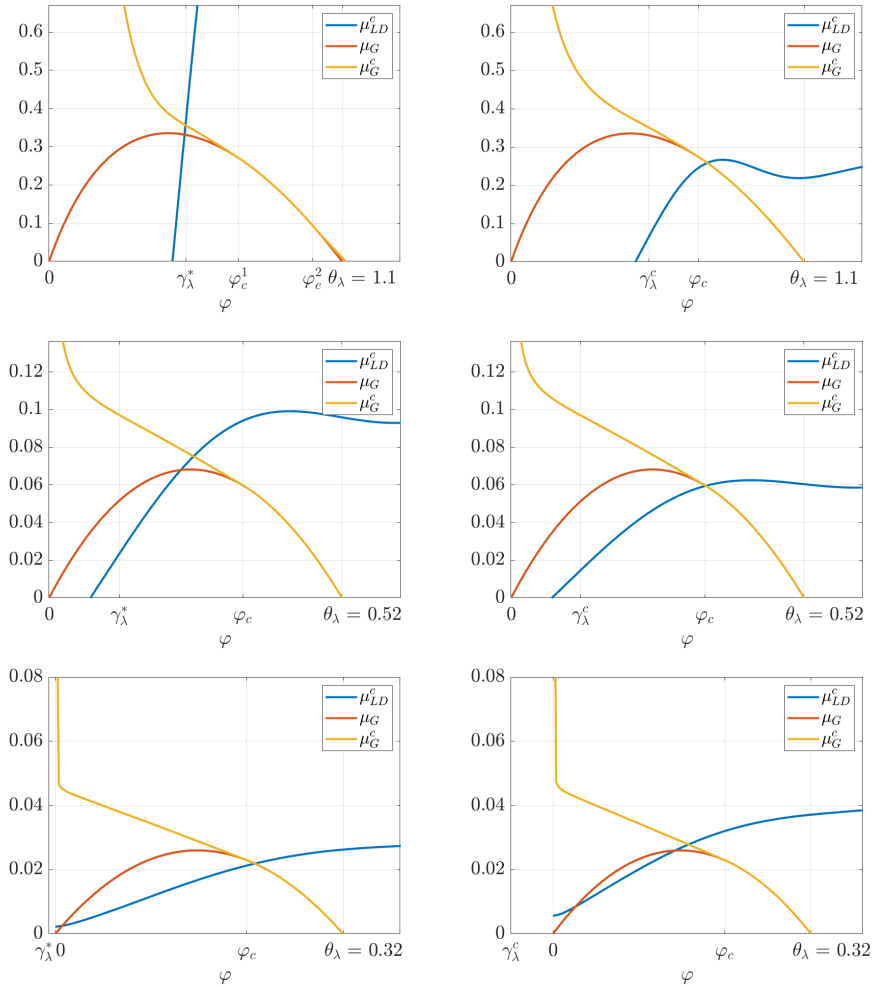

Figure 6.2: Graphs of the functions μ_{LD}^c, μ_G^c and μ_G for $\lambda = 0.5$ (top), $\lambda = 1.75$ (middle), $\lambda = 3$ (bottom). Left: $(\gamma_\lambda, c_\lambda) = (\gamma_\lambda^*, c_\lambda^*)$, right: $(\gamma_\lambda, c_\lambda) = (\gamma_\lambda^c, c_\lambda^c)$. The values of these parameters are given in Table 6.1. Note that these figures are similar to the scheme given in [22, Figure 3.27, p.126].

case gives rise to a situation where $\psi((a - a_c)_+) = \psi(0) = 0$, i.e., $\mu_G^c = \mu_G$, so that Theorem 4.1 applies. The results are presented in Figure 6.3.

In this test, the bisection algorithm does not always apply to cases where $a_c = 1$. Such situations may lead to multiple solution (see Section 3.3), and the initial interval cannot be defined a priori since the expression $\mu_L^c(\varphi) - \tan(\theta_\lambda - \varphi)\mu_D^c(\varphi) - \mu_G(\varphi)$ has the same sign on each boundary of I_0.

We observe that Algorithm 4.2 not only converges for all values of λ (as predicted by Theorem 4.1 for the case $a_c = 1$), but is in most cases more efficient than the other algorithms. In our tests, we always found that $\varepsilon = 1$ is the best choice in $[0, 1]$ in terms of rate of convergence.

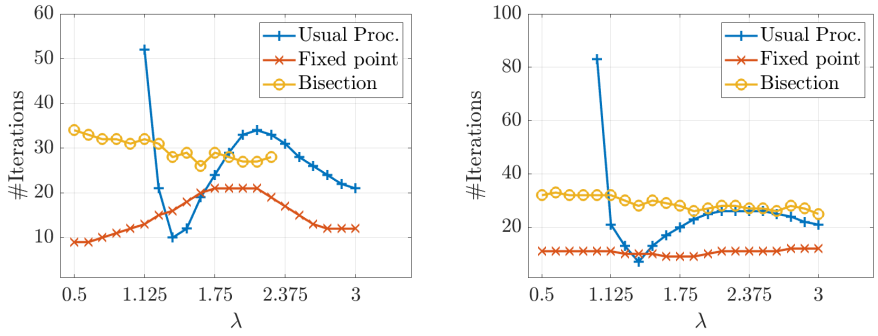

Figure 6.3: Number of iterations of Algorithm 4.1 (Usual Proc.), Algorithm 4.2 (Fixed-point) and Algorithm 4.3 (Bisection) algorithms required to solve Equation (3.10) according to the criterion (6.1) and for various values of λ. Only convergence cases are represented for usual algorithm, and cases of application for bisection algorithm. Left: $a_c = 1$, right: $a_c = 1/3$.

6.3. Optimization. We now use the gradient method presented in Algorithm 5.1 to compute optimal parameters $(\gamma_\lambda^c, c_\lambda^c)$ of (5.1) and compare it to the (explicit) optimal solution $(\gamma_\lambda^*, c_\lambda^*)$ associated with the simplified model given by Equations (5.2). The latter is used as an initial guess. The stopping criterion is $\|\nabla J_\lambda(\gamma_\lambda, c_\lambda)\| \leq$ Tol, with Tol$= 10^{-6}$. The results are presented in Figure 6.4. In this case, we

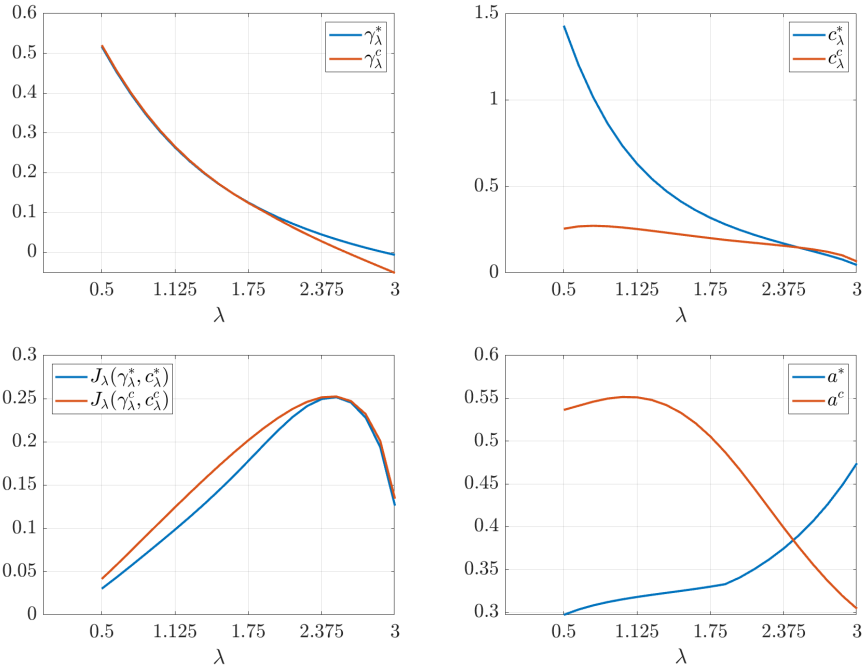

Figure 6.4: Graphs of the functions γ_λ^* and γ_λ^c, c_λ^* and c_λ^c, $J_\lambda(\gamma_\lambda^*, c_\lambda^*)$ and $J_\lambda(\gamma_\lambda^c, c_\lambda^c)$ and the corresponding values of a denoted by a^* and a^c, respectively.

find $C_P(\gamma_\lambda^c, c_\lambda^c) = 0.895654$ and $C_P(\gamma_\lambda^*, c_\lambda^*) = 0.837603$, so that the gradient proce-

dure enables to improve by 6.48% the performance in the framework of the corrected model. We also observe that the chord obtained with (5.2) is very large for small values of λ, which make its practical realization difficult. Note also that the behavior of a differs significantly according to whether one considers $(\gamma_\lambda, c_\lambda) = (\gamma_\lambda^*, c_\lambda^*)$ or $(\gamma_\lambda, c_\lambda) = (\gamma_\lambda^c, c_\lambda^c)$.

We finally test the existence of local maxima by plotting $J_\lambda(\gamma_\lambda^c, c_\lambda^c)$ on the domain $[-\theta_\lambda, \theta_\lambda] \times [0, 2]$. The results are represented in Figure 6.5.

We see that local maxima are present. However, they rather correspond to large values of c_λ, hence unrealistic solutions. The discontinuities that are observed for the case $\lambda = 0.5$ correspond to multiple solutions of Equation (3.10) (of types (2) and (3), see Section 3.3) which make the cost functional multivalued.

Acknowledgments. The authors acknowledge support from ANR Ciné-Para (ANR-15-CE23-0019) and ANR HyFloEFlu (ANR-10-IEED-0006-04).

Appendix: Convergence of Algorithm 4.1 in the simplified case. In the simplified case, Algorithm 4.1 can be summarized by an iterative procedure to compute a sequence $(\varphi^k)_{k\in\mathbb{N}}$ associated with the following recursion:

$$\varphi^{k+1} := \widetilde{f}(\varphi^k), \tag{6.2}$$

with $\widetilde{f}(x) := \frac{\pi}{2} - \operatorname{atan}(\lambda + \mu_L(x)h(x))$, $h(x) := \dfrac{\lambda \tan^{-1} x + 1}{\sin x}$.The stability can actually be obtained in the simplified case with additional assumptions.

LEMMA 6.1. *Suppose that* $\max I^+ = \theta_\lambda$, $\psi = 0$, *and that Assumption 1 holds, with* μ_L^c *non-decreasing. If*

$$\mu_L(\theta_\lambda) \le \mu_G(\gamma_\lambda). \tag{6.3}$$

and the initial value φ^0 *belongs to* $[\gamma_\lambda, \theta_\lambda]$, *then the sequence defined by* (6.2) *satisfies:*

$$\forall k \in \mathbb{N},\ \varphi^k \in [\gamma_\lambda, \theta_\lambda].$$

Proof. The result can be obtained by induction. Assume that for some $k \in \mathbb{N}$, $\varphi^k \in [\gamma_\lambda, \theta_\lambda]$. Because of (6.2), we have

$$\tan^{-1} \varphi^{k+1} := \lambda + \mu_L(\varphi^k)h(\varphi^k),$$

so that, since $\mu_L \ge 0$ and $\tan^{-1} \varphi^{k+1} \ge \lambda$. Definition (3.1) of θ_λ then implies that $\varphi^{k+1} \le \theta_\lambda$. On the other hand, thanks to the assumption (6.3), we have:

$$\tan^{-1} \varphi^{k+1} \le \lambda + \mu_L(\theta_\lambda)h(\gamma_\lambda).$$

Because of the assumption (6.3), the left-hand side of the previous inequality is bounded by $\tan^{-1} \gamma_\lambda$. The result follows. ∎

To get a sufficient condition for convergence, the later result must be completed by a contraction property. This is the purpose of the following lemma.

LEMMA 6.2. *Suppose that* μ_L *is differentiable and denote by* μ_L' *its derivative. The derivative of* $\widetilde{f}$ *satisfies*

$$-\sin\theta_\lambda \max_{I^+} \mu_L' h(\gamma_\lambda) \le \widetilde{f}'(\varphi) \le \sin\theta_\lambda \max_{I^+} \mu_L |h'(\gamma_\lambda)|.$$

Proof. Differentiating $\widetilde{f}$, we find that:

$$\widetilde{f}'(\varphi) = \frac{-1}{1 + (\lambda + \mu_L(\varphi)h(\varphi))^2}(\mu_L'(\varphi)h(\varphi) + \mu_L(\varphi)h'(\varphi)).$$

For $\varphi \in (\gamma_\lambda, \theta_\lambda)$, $\mu_L'(\varphi)h(\varphi) \geq 0$ and $\mu_L(\varphi)h'(\varphi) \leq 0$, we have

$$\frac{-1}{1 + (\lambda + \mu_L(\varphi)h(\varphi))^2}\mu_L'(\varphi)h(\varphi) \leq \widetilde{f}'(\varphi) \leq \frac{-1}{1 + (\lambda + \mu_L(\varphi)h(\varphi))^2}\mu_L(\varphi)h'(\varphi).$$

The result then follows from the facts that $\mu_L(\varphi)h(\varphi) \geq 0$ and that both h and h' are decreasing on $(\gamma_\lambda, \theta_\lambda)$. ∎

We are now in a position to obtain a conditional convergence result.

THEOREM 6.3. *In addition to the assumptions of Lemma 6.1, suppose that μ_L is differentiable and satisfies*

$$\sin\theta_\lambda \max_{I^+} \mu_L' h(\gamma_\lambda) \leq 1 \tag{6.4}$$

$$\sin\theta_\lambda \max_{I^+} \mu_L |h'(\gamma_\lambda)| \leq 1. \tag{6.5}$$

Then, if φ^0 belongs to $[\gamma_\lambda, \theta_\lambda]$, the sequence $(\varphi^k)_{k\in\mathbb{N}}$ defined by Equation (6.2) converges to the unique solution of Equation (3.4).

Proof. As a consequence of Lemma 6.1, the function $\widetilde{f}$ maps $[\gamma_\lambda, \theta_\lambda]$ onto itself. From Equations (6.4), (6.5) and Lemma 6.2 we deduce $\widetilde{f}$ is contracting. The result follows from the Banach fixed-point theorem. ∎

REFERENCES

[1] Y. Bazilevs, M. C. Hsu, I. Akkerman, S. Wright, K. Takizawa, B. Henicke, T. Spielman, and T. E. Tezduyar. 3D simulation of wind turbine rotors at full scale. Part I: Geometry modeling and aerodynamics. *International Journal For Numerical Methods In Fluids*, 65(1-3, SI):207–235, 2011.

[2] Y. Bazilevs, M. C. Hsu, J. Kiendl, R. Wuechner, and K. U. Bletzinger. 3D simulation of wind turbine rotors at full scale. Part II: Fluid-structure interaction modeling with composite blades. *International Journal For Numerical Methods In Fluids*, 65(1-3, SI):236–253, 2011.

[3] A. Betz. Das maximum der theoretisch möglichen ausnützung des windes durch windmotoren. *Zeitschrift für das gesamte Turbinenwesen*, 26:307–309, 1920.

[4] M. Bossy, J. Espina, J. Moricel, C. Paris, and A. Rousseau. Modeling the wind circulation around mills with a lagrangian stochastic approach. *The SMAI journal of computational mathematics*, 2:177–214, 2016.

[5] E. Branlard. *Wind turbine aerodynamics and vorticity-based methods: fundamentals and recent applications*. Research topics in wind energy. Springer, Cham, 2017.

[6] J. Buhl, M.L. New empirical relationship between thrust coefficient and induction factor for the turbulent windmill state. *Technical Report NREL/TP-500-36834*, 2005.

[7] T. Burton, D. Sharpe, N. Jenkins, and E. Bossanyi. *The Wind Energy Handbook*, volume 1. John Wiley and Sons, Ltd, 2001.

[8] M. Drela. Xfoil: An analysis and design system for low reynolds number airfoils. In T. J. Mueller, editor, *Low Reynolds Number Aerodynamics*, pages 1–12, Berlin, Heidelberg, 1989. Springer Berlin Heidelberg.

[9] L. Du, G. Ingram, and R. G. Dominy. A review of H-Darrieus wind turbine aerodynamic research. *Proceedings Of The Institution Of Mechanical Engineers Part C-Journal Of Mechanical Engineering Science*, 233(23-24, SI):7590–7616, 2019.

[10] W. Froude. On the elementary relation between pitch, slip and propulsive efficiency. *Trans. Roy. Inst. Naval Arch.*, 19(47):47–57, 1878.

[11] H. Glauert. The analysis of experimental results in the windmill brake and vortex ring states of an airscrew. *London: Aeronautical Research Committee*, 1026, 1926.

[12] H. Glauert. Airplane propellers. In W. F. Durand, editor, *Aerodynamic Theory*, volume 4, pages 169–360. Berlin: Julius Springer, 1935.
[13] H. Glauert. *The Elements of Aerofoil and Airscrew Theory*. Cambridge Science Classics. Cambridge University Press, 1983.
[14] M. O. Hansen. *Aerodynamics of Wind Turbines*. Taylor and Francis, 2015.
[15] B. D. Hibbs. Hawt performance with dynamic stall. Technical report, Solar Energy Research Institute, 1986.
[16] M.-C. Hsu and Y. Bazilevs. Fluid-structure interaction modeling of wind turbines: simulating the full machine. *Computational Mechanics*, 50(6, SI):821–833, 2012.
[17] N. Joukowsky. Vortex theory of screw propeller, i. *Trudy Otdeleniya Fizicheskikh Nauk Obshchestva Lubitelei Estestvoznaniya*, 16(1):1–31, 1912.
[18] N. Joukowsky. Windmill of the nej type. *Transactions of the Central Institute for Aero-Hydrodynamics of Moscow*, 1920.
[19] N. Joukowsky. Windmill of the nej type. *Joukowsky NE. Collected Papers, The Joukowsky Institute for AeroHydrodynamics, Moscow*, VI:405–409, 1937.
[20] F. Lanchester. A contribution to the theory of propulsion and the screw propeller. *Transactions of the Institution of Naval Architects*, 57:98–116, 1915.
[21] D. Maniaci. *49th AIAA Aerospace Sciences Meeting including the New Horizons Forum and Aerospace Exposition*, chapter An Investigation of WT_Perf Convergence Issues. Aerospace Sciences Meetings. American Institute of Aeronautics and Astronautics, 2011.
[22] J. Manwell, J. Mcgowan, and A. L Rogers. *Wind Energy Explained: Theory, Design and Application, Second Edition*, volume 30. John Wiley and Sons, Ltd, 2006.
[23] A. Ning, G. Hayman, R. Damiani, and J. M. Jonkman. Development and validation of a new blade element momentum skewed-wake model within aerodyn. In *Proceedings of the 33rd Wind Energy Symposium*, 2015.
[24] B. A. Prandtl L. Vier abhandlungen zur hydrodynamik und aerodynamik. *Göttinger Klassiker der Strömungsmechanik*, 3:1–100, 2010. (Flüssigkeit mit kleiner Reibung; Tragflügeltheorie, I. und II. Mitteilung; Schraubenpropeller mit geringstem Energieverlust).
[25] W. J. M. Rankine. On the mechanical principles of the action of propellers. *Trans. Roy. Inst. Naval Arch.*, 6:13–30, 1865.
[26] A. P. Schaffarczyk. *Introduction to wind turbine aerodynamics*. Green Energy and Technology. Springer, Dordrecht, 2014.
[27] W. Shen, R. Mikkelsen, J. Sorensen, and C. Bak. Tip loss corrections for wind research turbine computations. *Wind Energy*, 8(4):457–475, 2005.
[28] Q. Song and W. D. Lubitz. Bem simulation and performance analysis of a small wind turbine rotor. *Wind Engineering*, 37(4):381–399, 2013.
[29] J. Sørensen. *General Momentum Theory for Horizontal Axis Wind Turbines*. Springer, 2016.
[30] D. Spera, editor. *Wind Turbine Technology: Fundamental Concepts in Wind Turbine Engineering, Second Edition*. ASME, New York, NY, 2009.
[31] G. A. M. van Kuik. The Lanchester-Betz-Joukowsky limit. *Wind Energy*, 10(3):289–291, 2007.
[32] R. E. Wilson, P. B. S. Lissaman, and S. N. Walker. Aerodynamic performance of wind turbines. final report. Technical report, Oregon State University, 1976.

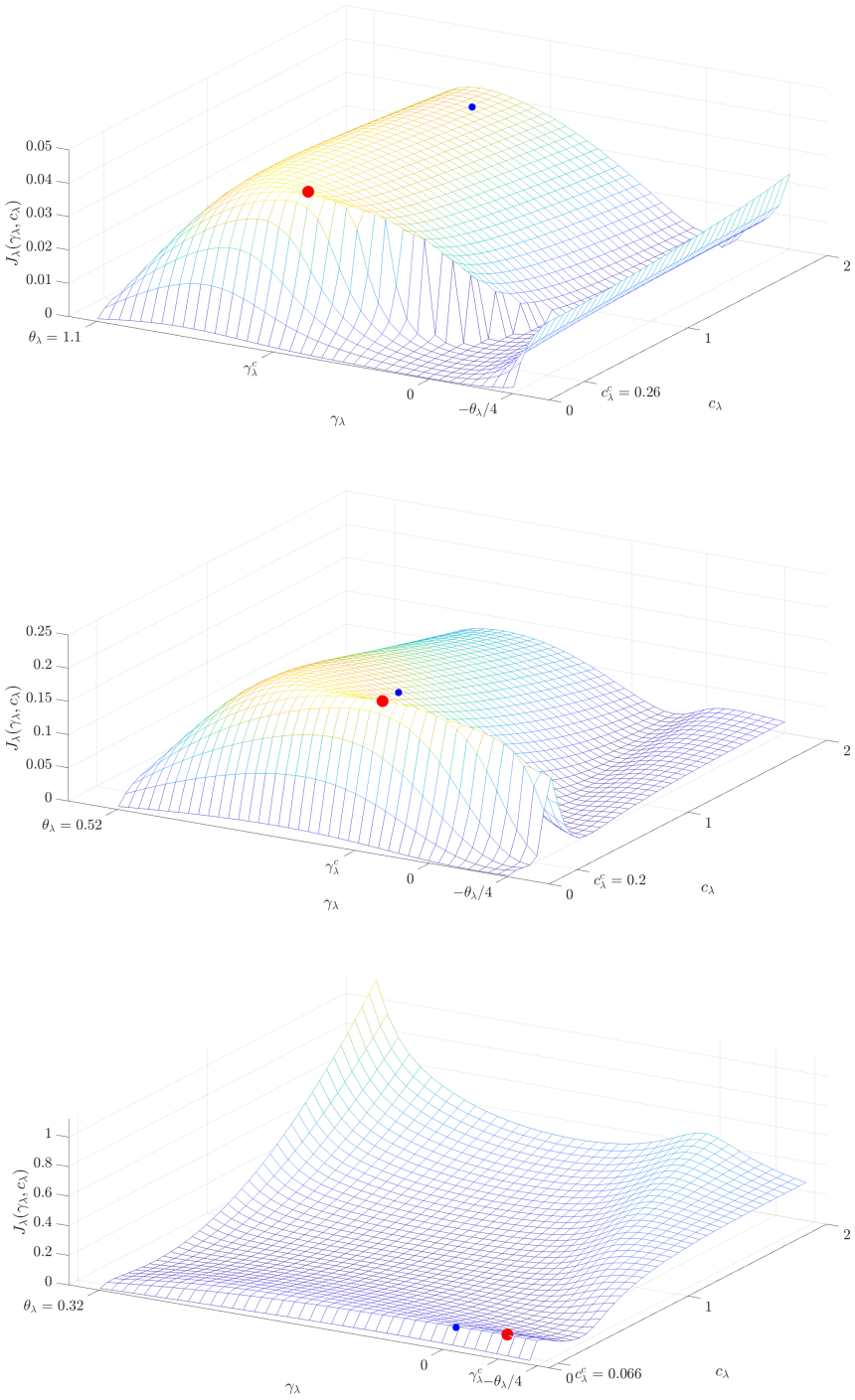

Figure 6.5: Graphs of the functions $(\gamma_\lambda, c_\lambda) \mapsto J_\lambda(\gamma_\lambda, c_\lambda)$ (left) for $\lambda = 0.5$ (top), $\lambda = 1.75$ (middle), $\lambda = 3$ (bottom). The large red point and the small blue point indicate locations of $(\gamma_\lambda^c, c_\lambda^c)$ and $(\gamma_\lambda^*, c_\lambda^*)$, respectively. See the values of these parameters in Table 6.1.